Geophysical Journal International

Geophys. J. Int. (2012) **188,** 798–818 doi: 10.1111/j.1365-246X.2011.05307.x

The eastern Jan Mayen microcontinent volcanic margin

Asbjørn Johan Breivik,[1] Rolf Mjelde,[2] Jan Inge Faleide[1] and Yoshio Murai[3]

[1] *Department of Geosciences, P.O. Box* 1047 *Blindern, University of Oslo,* N-0316 *Oslo, Norway. E-mail: a.j.breivik@geo.uio.no*
[2] *Department of Earth Science, Allégt* 41, *University of Bergen,* N-5007 *Bergen, Norway*
[3] *Institute of Seismology and Volcanology, Hokkaido University,* N10 W8 *Kita-ku, Sapporo* 060-0810, *Japan*

Accepted 2011 November 15. Received 2011 November 3; in original form 2011 July 1

SUMMARY

The Jan Mayen microcontinent (JMMC) in the NE Atlantic was created through two Cenozoic rift episodes. Originally part of East Greenland, the JMMC rifted from NW Europe during the Early Eocene under extensive magmatism. The eastern margin is conjugate to the Møre–Faeroes volcanic margin. The western JMMC margin underwent prolonged extension before it finally separated from East Greenland during the Late Oligocene. Here we present the modelling by forward/inverse ray tracing of two wide-angle seismic profiles acquired using Ocean Bottom Seismometers, across the northern and the southern JMMC. Early Eocene breakup magmatism at the eastern JMMC produced an igneous thickness of 7–9 km in the north, and 12–14 km in the south. While the continent is clear in the north, the southern JMMC appears to be affected by later Icelandic magmatism. Reduced seismic velocity and increased crustal thickness are compatible with continental crust adjacent to the volcanic margin in the south, but the continental presence towards the Iceland shelf is less clear. Our magnetic track off the southern JMMC gives seafloor spreading rates comparable to that of the conjugate Møre Margin. Transition to ultraslow seafloor spreading occurs at ∼43 Ma, indicating onset of major deformation of the JMMC. Calculating the igneous thickness—mean V_P relationship at the eastern volcanic margin gives the typical positive correlation seen elsewhere on the NE Atlantic margins. The results indicate temperature driven breakup magmatism under passive mantle upwelling, with a maximum mantle temperature anomaly of ∼50 °C in the north and 90–150 °C in the south.

Key words: Controlled source seismology; Continental margins: divergent; Oceanic plateaus and microcontinents; Large igneous provinces; Crustal structure; Magma genesis and partial melting.

1 INTRODUCTION

The Jan Mayen Ridge (JMR) is a north-trending bathymetric feature in the Norwegian–Greenland Sea (Fig. 1). While the northern part consists of a single ridge, south of the Jan Mayen Trough there are several smaller ridges. Early studies of the JMR pointed out its role as a microcontinent (the Jan Mayen microcontinent: JMMC), first rifted off the Norwegian Margin with Greenland, and then off Greenland itself (Talwani & Eldholm 1977). Later studies further investigated the structure and volcanism of the ridge (e.g. Myhre *et al.* 1984; Skogseid & Eldholm 1987; Gudlaugsson *et al.* 1988). Seaward dipping reflectors observed on the eastern margin are similar to features on the mid-Norwegian margin (Skogseid & Eldholm 1987), where Ocean Drilling Program wells penetrated basalt flows deposited during breakup (e.g. Planke 1994). The conjugate margin is the volcanic Møre Margin off mid-Norway, where seafloor spreading initiated at ∼54 Ma on the Aegir Ridge (e.g. Berndt *et al.* 2001; Torsvik *et al.* 2001; Lundin & Doré 2002).

Seafloor spreading on the Aegir Ridge became magma starved soon after the initial pulse of breakup magmatism (Breivik *et al.* 2006). There was also less breakup magmatism in the north than in the south on the Møre Margin (Berndt *et al.* 2001). The Aegir Ridge became extinct around (∼25–28 Ma), when the JMMC rifted off east Greenland and oceanic spreading shifted to the presently active Kolbeinsey Ridge (Vogt *et al.* 1980; Nunns 1983; Mjelde *et al.* 2008a). Continental stretching commenced at least 20 Myr before Late Oligocene breakup occurred in the Jan Mayen Basin, and the structure is dominated by the rifting from Greenland, with many of the major normal faults facing westwards (Gudlaugsson *et al.* 1988; Kuvaas & Kodaira 1997). The northwestern part of the JMMC has been mapped by regional Ocean Bottom Seismometer data (OBS), documenting the Late Oligocene non-volcanic, passive margin development (Kodaira *et al.* 1998; Mjelde *et al.* 2007). The limit of the JMMC to the south is unclear, as the bathymetric ridges disappear, and the bathymetry rises towards the Iceland shelf (Fig. 1).

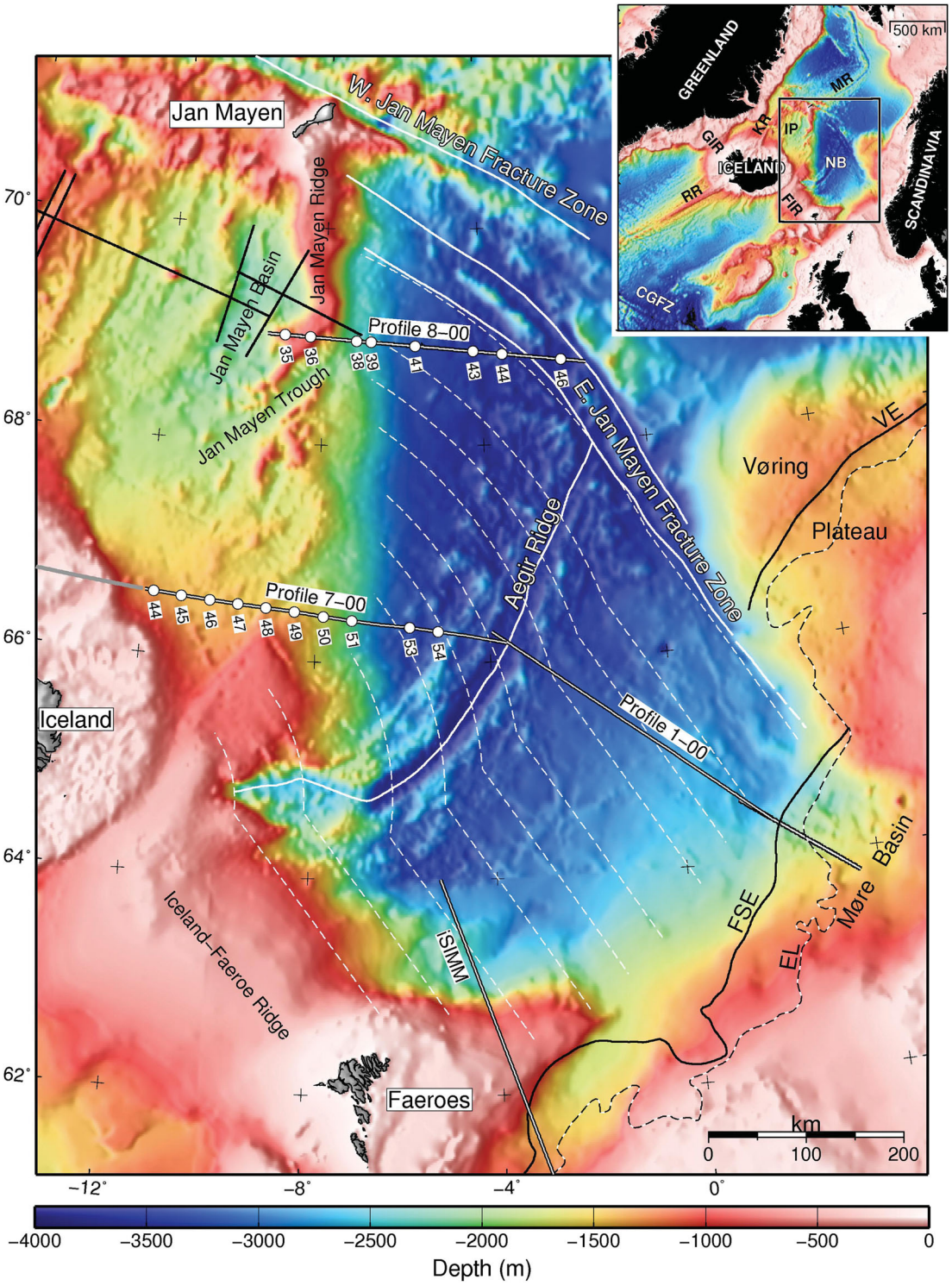

Figure 1. Location of Profile 8-00 and 7-00, with numbered OBS locations on IBCAO/GEBCO bathymetry (Jakobsson *et al.* 2008). The profiles west of profile 8-00 and east of profile 7-00 are discussed by Kodaira *et al.* (1998) and Breivik *et al.* (2006), respectively. The iSIMM profile is discussed by Parkin *et al.* (2007), Parkin & White (2008) and White *et al.* (2008). The Norway Basin flowlines (dashed, white lines) are from Breivik *et al.* (2006). From Skogseid & Eldholm (1987): EL, Eastern limit Eocene lavas; FSE, Faeroe-Shetland Escarpment; VE, Vøring Escarpment. Index map: CGFZ, Charlie-Gibbs Fracture Zone; FIR, Faeroe-Iceland Ridge; GIR, Greenland-Iceland Ridge; IP, Iceland Plateau; KR, Kolbeinsey Ridge; MR: Mohn Ridge; NB, Norway Basin; RR, Reykjanes Ridge.

This paper describes the traveltime modelling of two OBS profiles acquired across the western Norway Basin and the JMMC/Iceland Plateau. In addition, we use magnetic track data collected with the OBS profiles to constrain early seafloor spreading rates and magmatic productivity. Profile 8-00 in the north is near conjugate to an OBS profile at the Møre margin (Breivik *et al.* 2006, Fig. 1), while Profile 7-00 is just north of conjugate to the iSIMM OBS profile at the northern Faeroes Margin (White *et al.* 2008, Fig. 1).

We will present our profiles in light of recent results from the conjugate margin. The regional discussion of the JMMC extent will also make use of satellite-derived gravity (Andersen *et al.* 2008), as well as ship/flight track derived magnetic maps (Verhoef *et al.* 1996; Gernigon *et al.* 2009).

2 DATA ACQUISITION AND PROCESSING

The survey was performed during the summer of the year 2000, by the R/V Håkon Mosby of the University of Bergen. The project has been conducted in collaboration between the Department of Earth Science, University of Bergen, the Norwegian Petroleum Directorate (NPD), and the Institute of Seismology and Volcanology (ISV), Hokkaido University, Sapporo. An array consisting of four equal sized Bolt air guns with a total volume of 78.66 l (4800 in.^{3}) were fired every 200 m for each OBS profile, and the data were recorded by ISV three-component OBSs with analog or digital recording. A total of eight OBSs containing good data were recovered for Profile 8-00 (330 km long), while three OBSs failed. Profile 7-00 (380 km long) presented here is part of a longer profile continuing north of Iceland (Brandsdóttir *et al.* 2008). One instrument failed on the eastern part, while 10 OBSs returned good data sets.

The pre-processing consists of linear clock drift correction, extracting a 60 s record length for each shot, and linking to navigation. OBS positions are also corrected for drift along line where this is apparent. Navigation was performed by a differential global positioning system. The OBS data processing shown in the figures consists of a 5–12 Hz bandpass filter, offset-dependent amplitude scaling and spiking deconvolution. The *P*-wave data time axis is reduced by a velocity of 8.0 km s^{-1}. Surface seismic data were recorded by an analogue, single channel streamer for both profiles. Magnetic data were logged every 5 s by a GeoMetrics G-801 proton precession magnetometer towed 180 m behind the ship. Magnetic processing consists of repositioning, adjusting for short-term field fluctuations from base stations in Leirvogur, Iceland and Jan Mayen, and correcting to the International Geomagnetic Reference Field (IGRF-11). The geomagnetic field was quiet during the recording period, and the quality of the data good.

3 *P*-WAVE MODELLING

The *P*-wave data, recorded by the OBS vertical components, were modelled by forward/inverse ray tracing software (Zelt & Smith 1992). The model is solved layer by layer from top to bottom. The inversion routine is best used on a limited number of depth and/or velocity nodes from a single layer covered by several OBS data sets, and is routinely used for solving deeper layers. The software also evaluates the goodness of fit between interpreted and modelled traveltimes using χ^2 analysis. The χ^2 value weighs the mismatch between observed and calculated arrival times by the estimated interpretation uncertainty, so that a value of 1 or lower per phase signifies a fit. The main uncertainty in interpretation may come from the difficulty to pick the first onset of an arrival. For the short offset arrivals from the sedimentary layers and uppermost crust the uncertainty is estimated to $\pm$50 ms, while later arrivals originating deeper are assigned an uncertainty of $\pm$100 ms. A few indistinct arrivals have been assigned a greater uncertainty.

Profile 8-00 crosses the northern JMR and the oceanic basin to the East Jan Mayen Fracture Zone (EJMFZ, Fig. 1). Profile 7-00 was acquired across the southern JMMC/Iceland Plateau, and covers the oceanic basin to the Aegir Ridge (Fig. 1). The quality of the recorded data is very good for both profiles. The complete *P*-wave data with models are shown in the Supporting Information section of this paper. The single channel seismic (SCS) reflection lines were used to construct initial models, where the top of the oceanic crust stands out clearly along most parts of the profiles, but no details can be seen below that (Fig. 2). Sedimentary velocities are low, and only return identifiable refracted waves on a few OBSs, but there are numerous reflections from the top of the basement. Both indicate a sedimentary velocity below $\sim$2 km s^{-1} for the two uppermost layers, except for near the Iceland shelf in the south.

The uppermost layers are densely parametrized by depth nodes, where the echo sounding and SCS data constrain water depth and near-surface structure. Typical node spacing is 2–4 km for upper layers, while it is mostly 10–30 km for the lower layers within the basement and for the Moho. Velocity nodes are fewer, usually spaced 20–50 km apart for the whole model. The sedimentary layers have poor velocity control, and have very few velocity nodes. Reflections that could not be tied to the velocity layer boundaries were fitted by introducing floating reflectors, visible as short lines in the figures. Labelled phase codes are: P_x sedimentary refraction, P_{g1} upper basement refraction, P_{g2} middle basement refraction, P_{g3} and P_{g4} lower basement refractions, P_n upper-mantle refraction, P_GP intra-basement reflection, P_MP Moho reflection and P_FP upper-mantle reflection.

3.1 Profile 8-00: the northern Jan Mayen microcontinent

The JMMC is constrained by OBSs 35–41 (Fig. 1). The vertical component data for OBSs 35 and 39, together with the model ray tracing and the traveltime fit, are presented in Figs 3 and 4. The velocity model is shown in Fig. 5. See Supporting Information for all data and models. Profile 8-00 is close to the older OBS Profile 4–95 located 10–30 km to the north (Kodaira *et al.* 1998). The older profile covers the western and central parts of the JMMC, but not the eastern margin. Both profiles show an asymmetric crustal root underneath the bathymetric ridge, with the thickest crust displaced to the eastern side (Fig. 5). They also show a thickness of 0.5–1.5 km of sediments draping the ridge, and a faulted relief of sedimentary rocks underneath. The large westward facing normal fault seen in the SCS profile on the eastern flank at $\sim$60 km distance has a throw of $\sim$0.5 s two-way time (TWT, Fig. 2), corresponding to $\sim$500 m. The effect of the fault is also seen in a distinct offset of the seismic arrival times above it on the OBS data (Figs 3 and 4), agreeing very well with this throw. It involves most strata up to near seafloor, and may therefore belong to the faults created by the separation of the JMMC from East Greenland.

Earlier studies based on multichannel seismic reflection (MCS) data indicate that there is a basaltic layer on the eastern JMMC flank in the north, often associated with seafloor dipping reflectors (Myhre *et al.* 1984; Skogseid & Eldholm 1987; Gudlaugsson *et al.* 1988). Kodaira *et al.* (1998) included an $\sim$1-km-thick layer of basalts in their OBS model, though the thickness was unconstrained by the OBS data due to velocity inversion underneath. Profile 8-00 lacks a layer with a velocity near what they found (4.6–4.8 km s^{-1}) and there is no sign of a velocity inversion (Fig. 5), thus we cannot identify it. Crystalline basement with *P*-wave velocity above 6 km s^{-1} was found at depths between 4 and 6 km within the ridge. The model of Kodaira *et al.* (1998), 30 km to the north, indicates up to $\sim$5–6-km-thick sedimentary rocks within the ridge west of our model.

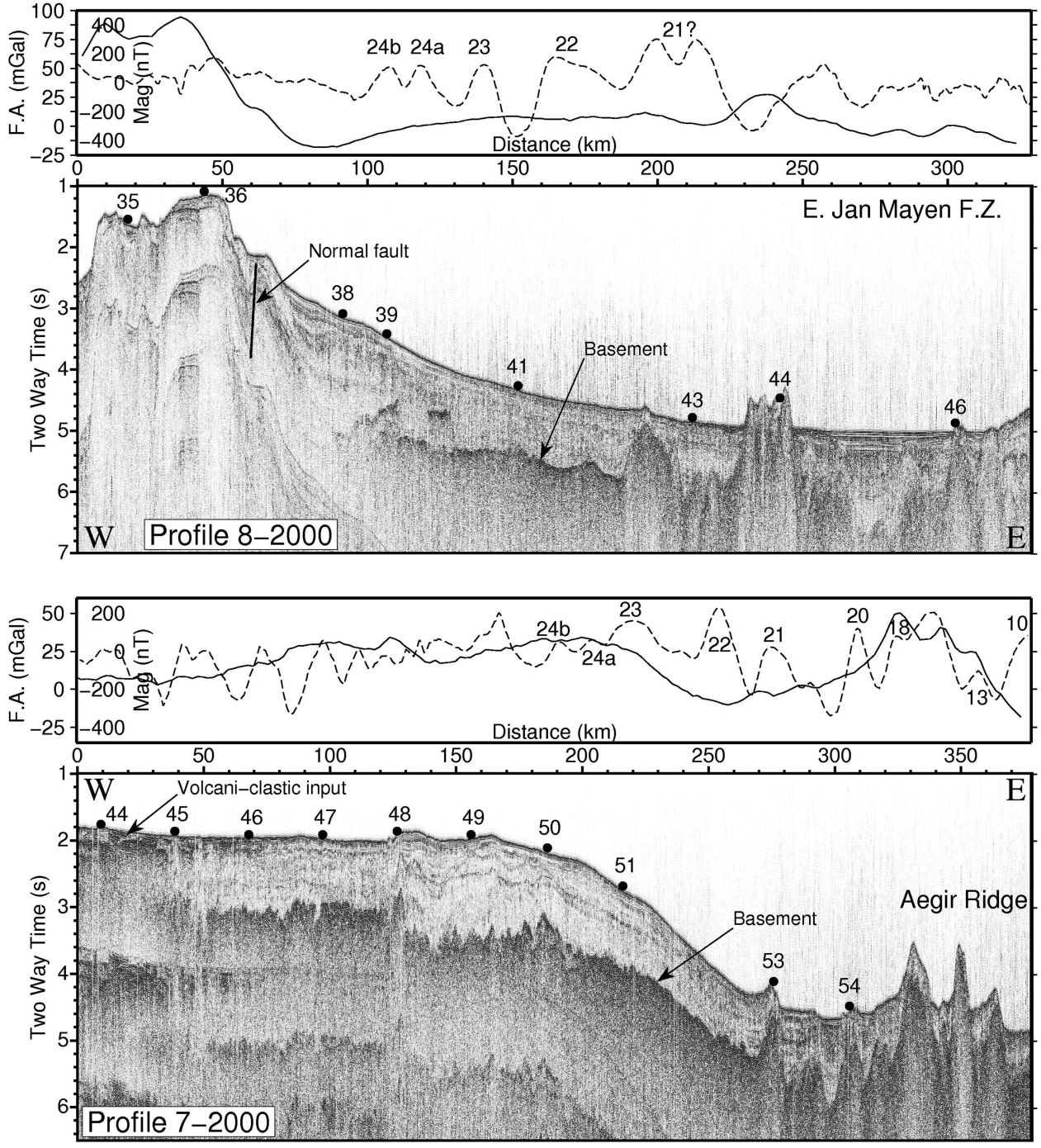

Figure 2. Single channel streamer reflection data recorded with OBS Profile 8-00 (upper) and Profile 7-00 (lower), shown in two-way time (TWT). Numbered black dots represent OBS locations. Coincident gravity (Andersen *et al.* 2008) and magnetic data (this study) are shown above each seismic section. Magnetic: dashed line, gravity: solid line.

Maximum Moho depth is 16.6 km (Fig. 5), compared to 19.7 km of the older profile located 25 km farther to the north. Both profiles show lower crustal velocity above 6.7 km s^{-1} under the JMR, while our profile documents further velocity increase to more than 7 km s^{-1} to the east. This velocity continues into the lower oceanic crust, indicating a gabbroic composition. The transition between this and the continental crust farther west is gradual, which could indicate a zone of magmatic intrusions into the lower continental crust, similar to that of the iSIMM profile north of the Faeroes (White *et al.* 2008). This could also offer an explanation for the asymmetry between the bathymetry and the Moho relief, as a gabbroic lower crust would be stronger than the more quartz-rich lithology, which the lower velocities indicate farther west. Thus the volcanic margin would sustain less tectonic deformation.

The oceanic crust is 5–5.5 km thick (Fig. 5), comparable to that of oceanic crust near the Norwegian Møre Margin (Breivik *et al.* 2006).

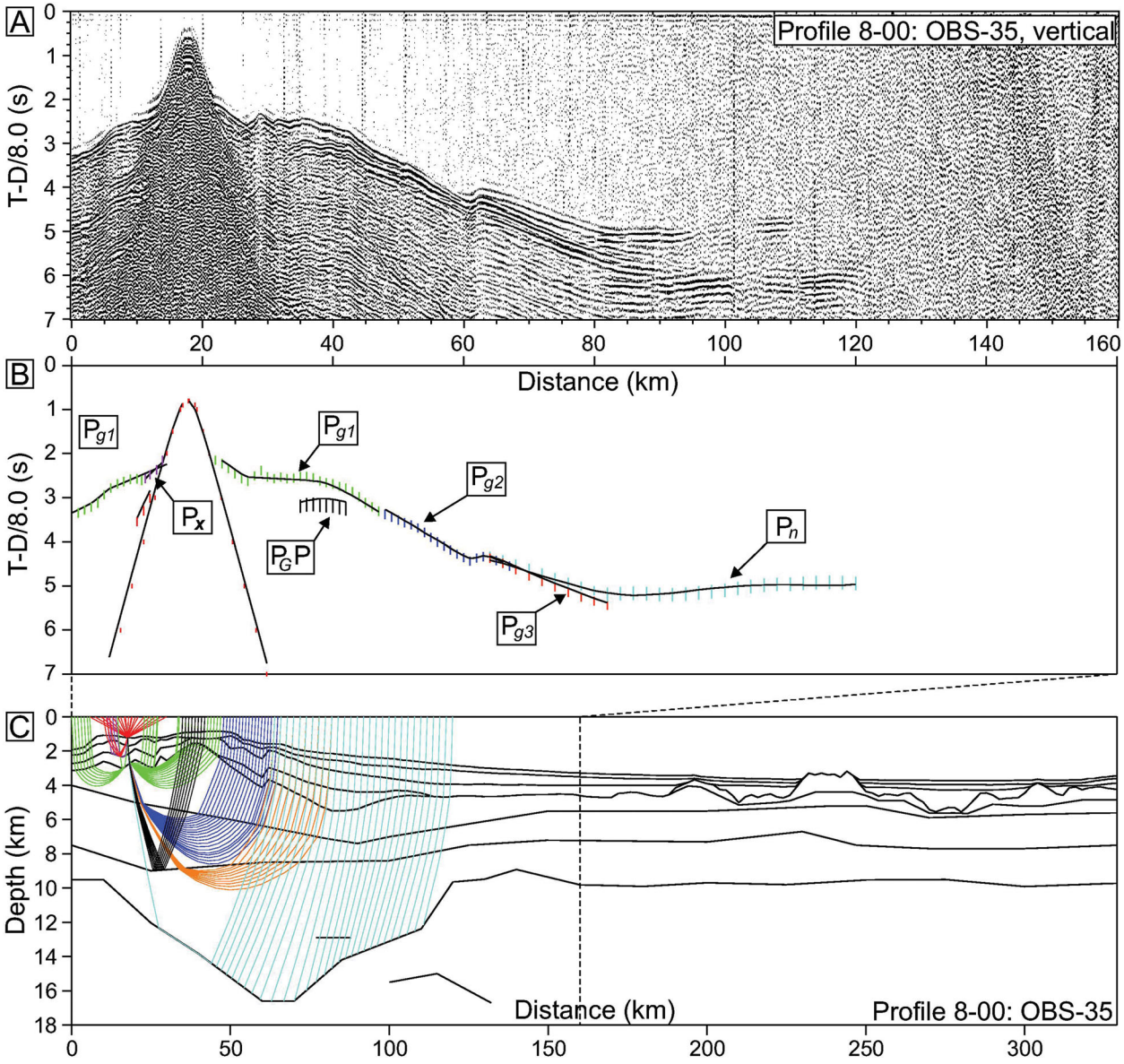

Figure 3. Data, interpretation and ray tracing of OBS 35, Profile 8-00, northern Jan Mayen microcontinent. (A) OBS data, vertical component. (B) Interpretation and model reproduction. (C) Ray tracing of the velocity model.

The velocity structure of the upper oceanic crust is well constrained by the OBS data. The top is smooth near the JMMC, and the velocity of the upper oceanic crust fairly high (∼5.5 km s^{-1}) compared to normal (White *et al.* 1992). The top basement becomes rougher and the oceanic layer 2 velocity decreases towards the EJMFZ. The EJMFZ itself forms a deep trough in the basement, but there is no Moho relief or velocity signature of it in the lower crust.

3.2 Profile 7-00: the southern Jan Mayen microcontinent

The profile presented here is part of a longer profile extending onto the Icelandic shelf (Fig. 1). The SCS profile shows top basement well for most of the profile, except for the westernmost 40 km, where there is a zone of strong reflectivity within the sediments (Fig. 2). We interpret this to be volcani-clastic material derived from the Icelandic shelf located 20 km to the west. The sedimentary thickness is between 1 and 1.5 km. For most of the profile the velocity is below 2 km s^{-1}, but it increases slightly in the volcaniclastic part. Data with the model ray tracing and the traveltime fit for OBSs 48, 50 and 54 are shown in Figs 6–8, and the velocity model in Fig. 9. See Supporting Information for all data and models.

While top basement in the west is reflective both in the SCS and the OBS data, refracted first arrivals appear not to come from the top basement here, but from a layer at 3–4 km depth. Constraints of the uppermost basement velocity are mainly by the delay of later phases, indicating 2.8–3.5 km s^{-1}. The top basement velocity becomes higher (4–5 km s^{-1}) from OBS 48 and eastwards, from where top basement reflections and refractions come from the same level. Middle crustal velocities are well constrained by refracted first arrivals for the whole model.

The Moho is constrained at 15–18 km depth by reflections (P_MP) and a few refractions through the uppermost mantle (P_n). There are two ∼30-km-wide areas with marked Moho reliefs between 60 and

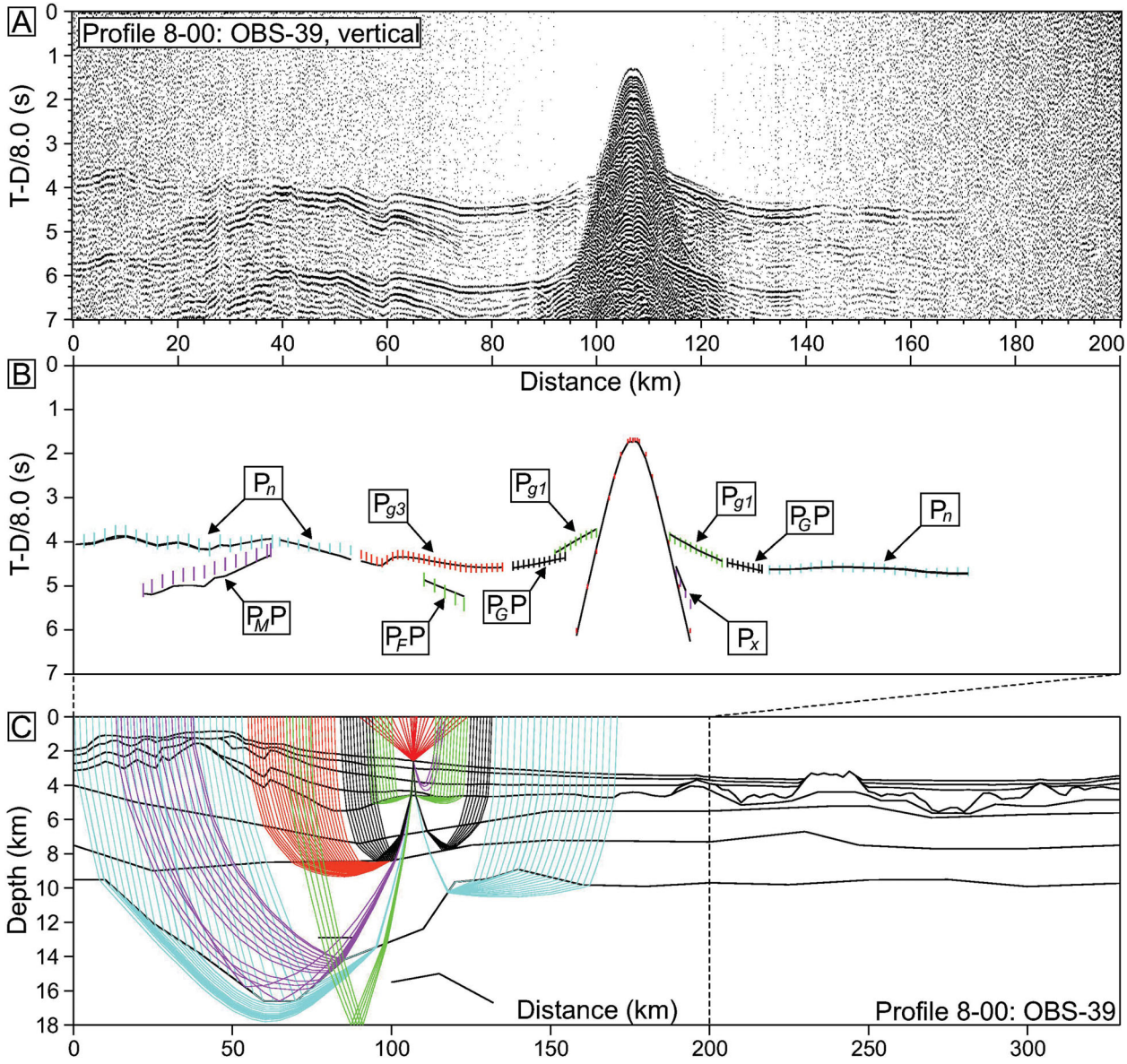

Figure 4. Data, interpretation and ray tracing of OBS 39, Profile 8-00, northern Jan Mayen microcontinent. (A) OBS data, vertical component. (B) Interpretation and model reproduction. (C) Ray tracing of the velocity model.

190 km in the model. The eastern Moho structure is well constrained by OBSs 48–50 (Figs 6 and 7), and has a relief of up to 3.5 km over adjacent areas. The velocity of the middle and lower crust is well controlled in this part of the model by diving waves. The velocity falls from ∼7.0 s^{-1} to 6.8–6.9 km s^{-1} above the deepest part of the Moho, also corresponding to a fall in gravity, both indicating a slight compositional change (Fig. 9).

There is a zone with a smooth Moho topography between 180 and 280 km in the model, where the crust thins into the Norway Basin. This is well constrained by OBSs 49–54 (Figs 7 and 8). The internal velocity structure is smoother than in the crust farther west, and the velocity at the bottom of the crust reaches 7.2–7.3 km s^{-1}. This area greatly resembles the volcanic Vøring and Møre Margins on the Norwegian side (e.g. Mjelde *et al.* 2005; Breivik *et al.* 2006, 2009), and was similarly created by the extensive breakup magmatism, producing a maximum igneous crustal thickness of ∼12 km immediately after breakup.

The easternmost 100 km of the model covers thin oceanic crust (4–6 km) towards the extinct Aegir Ridge. The structure is typical for very slow spreading ridges, with thin crust and rough basement topography (Malinverno 1991; Dick *et al.* 2003). The eastern end of the profile ties to OBS Profile 1-00 (Breivik *et al.* 2006), where both profiles indicate reduced crustal velocities within the Aegir Ridge crust itself.

3.3 Uncertainties and resolution

The precision of seismic models is hard to quantify, as it will eventually depend on a somewhat subjective evaluation of the accuracy of the data and interpretation. Since we want to study the volcanic margin in particular, we target this part located between 180 and 280 km of Profile 7-00. The breakup magmatism is much greater here than at Profile 8-00 in the north, and is therefore the most important

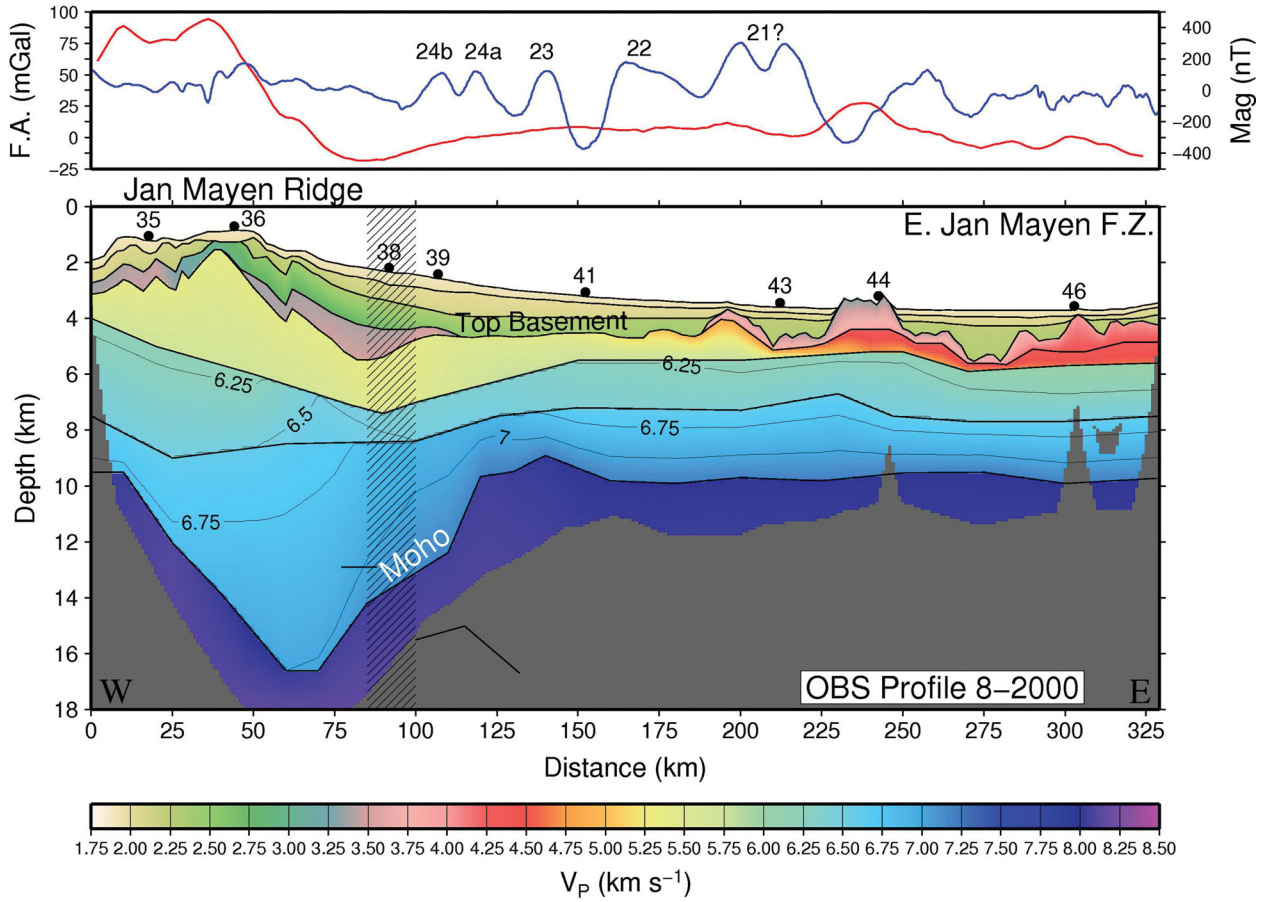

Figure 5. Gridded crustal velocity model for Profile 8-00. The parts of the model not covered by *P*-wave rays are masked. Rays from floating reflectors do not constrain velocity and are not included in the ray coverage. The OBS locations are numbered on the seafloor. Hachure indicates the continent–ocean transition. Both gravity (red line) (Andersen *et al.* 2008) and magnetic anomalies (blue line) with anomaly identifications are shown in the panel above.

part of the models if we are to constrain the mantle melting process. The analysis depends on the trade-off between lower crustal velocity and the Moho depth. Higher lower-crustal velocity can be accommodated by increased Moho depth and still produce a reasonable fit for relevant phases. The lower crustal bulk velocity and Moho depth nodes are therefore treated as two groups, and depths or velocities within each group are changed iteratively by the same amount. For each iteration within one group, the other group goes through all iterations for a specified interval. This approach gives a good indication of the minimum and maximum velocity models the data will support. Using P_{g4}, P_MP and P_n phases between 180 and 280 km in the model, 1683 different models were run and the fit statistics extracted. Fig. 10 shows the contoured χ^2 and rms ΔT fit summary for these model runs. Loss of the ability to trace rays to the observed picks limit the model space further, and is indicated by the background shading. Defined between $\chi^2 \leq 1$ and few rays lost, the Moho depth has an uncertainty of -0.2 km to $+1.4$ km, and the lower crustal velocity an uncertainty of -0.12 km s^{-1} to $+0.15$ km s^{-1}.

Fit statistics indicate the ease of picking arrivals, and the accuracy of the model reproduction for the targeted region. The ray coverage density will in addition indicate which parts of the model are best constrained. We show ray hit counts for 2.5 × 0.25 km (distance-depth) grid cells for each model in Fig. 11. For Profile 8-00 in the north, there is good ray coverage both in the upper, middle and lower part of the JMMC. Profile 7-00 in the south has best coverage at mid-crustal levels, but also good lower crustal coverage where the crust is thickest, and of the volcanic margin. The uppermost crust of the margin and the oceanic crust have less coverage.

4 POTENTIAL FIELD DATA

4.1 Gravity maps

The free-air gravity map is derived from satellite altimetry measurements, gridded at 1′ (arc-minute) cells (Andersen *et al.* 2008; Andersen & Knudsen 2009, Fig. 12B). There is a good correlation between bathymetric relief and the gravity anomalies (Figs 12A and B). Profile 8-00 crosses the southernmost part of the prominent, positive gravity anomaly of more than 90 mGal over the northern JMR (Figs 5 and 12B). East of that, most of the profile has subdued gravity anomalies, before it terminates at the negative anomalies over the EJMFZ. The low to the west of the JMR corresponds to highly stretched continental crust, which is thinner than the oceanic crust farther to the west (Kodaira *et al.* 1998, Fig. 13).

The gravity minimum on Profile 7-00 is -19 mGal, located over the Aegir Ridge valley, while the maximum of 50 mGal is over the Aegir Ridge axial mountains (Figs 9 and 12B). The area south of the Jan Mayen Trough shows several smaller bathymetric ridges having positive gravity signatures, mostly to the north of Profile 7-00. There is a NE-trending, weakly negative anomaly south of

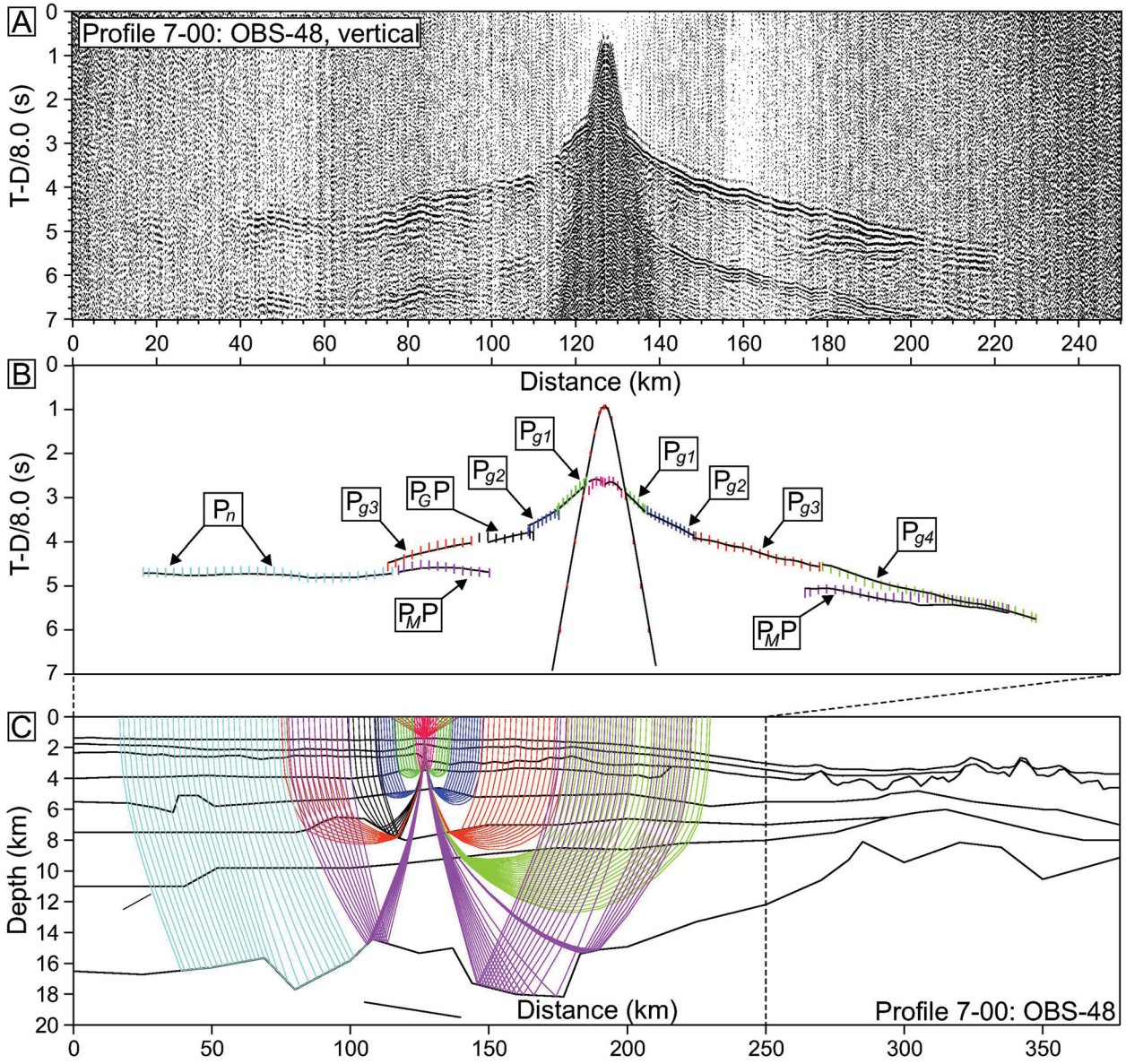

Figure 6. Data, interpretation and ray tracing of OBS 48, Profile 7-00, southern Jan Mayen microcontinent/Iceland Plateau. (A) OBS data, vertical component. (B) Interpretation and model reproduction. (C) Ray tracing of the velocity model.

these ridges, resembling the Jan Mayen Trough signature to the north. Profile 7-00 crosses this obliquely between OBSs 48 and 49 (Fig. 9). The gravity minimum lies between the two deepest Moho parts, and appears related to reduced middle- and lower crustal velocity, indicating reduced density (Ludwig *et al.* 1970).

Using a Bouguer plate approximation with a density of 2670 kg m^{-3}, the Bouguer correction was calculated for each grid cell (1 arc-minute, Fig. 12C). Since no terrain corrections were applied, the result is a Simple Bouguer gravity map. This map highlights variations in Moho depth across the study area. Still, even if the crust was homogeneous, the Moho depth cannot be calculated directly from the Bouguer gravity without correcting for the thermal/density structure of the mantle (Greenhalgh & Kusznir 2007).

The thin oceanic crust/shallow mantle in the Norway Basin gives high Bouguer gravity values. The boundary between the oceanic basin and the JMMC volcanic margin shows as a N–S oriented gradient going from the West Jan Mayen Fracture Zone (WJMFZ) in the north down to the tip of the Aegir Ridge in the south. The northern JMR shows reduced gravity following the extent of the bathymetric ridge (Fig. 12C), and the thin crust of the continental Jan Mayen Basin to the west (Kodaira *et al.* 1998) shows high anomalies. There is no clear gradient at the western side of the JMMC: The oceanic crust created at the Kolbeinsey Ridge north of Iceland is thicker than the world average (Kodaira *et al.* 1997), the lithosphere younger and hotter, and hence the Bouguer gravity is lower than in the Jan Mayen and Norway basins. The Bouguer gravity is low around Iceland where the crust is thick. Judging from the Bouguer map, Icelandic crustal growth may reach the area of Profile 7-00, likely contributing to the crustal thickness in the west.

4.2 Magnetic anomalies

Recent aeromagnetic surveys cover the EJMFZ (Gernigon *et al.* 2009) and the eastern Norway Basin (Olesen *et al.* 2010; Gernigon

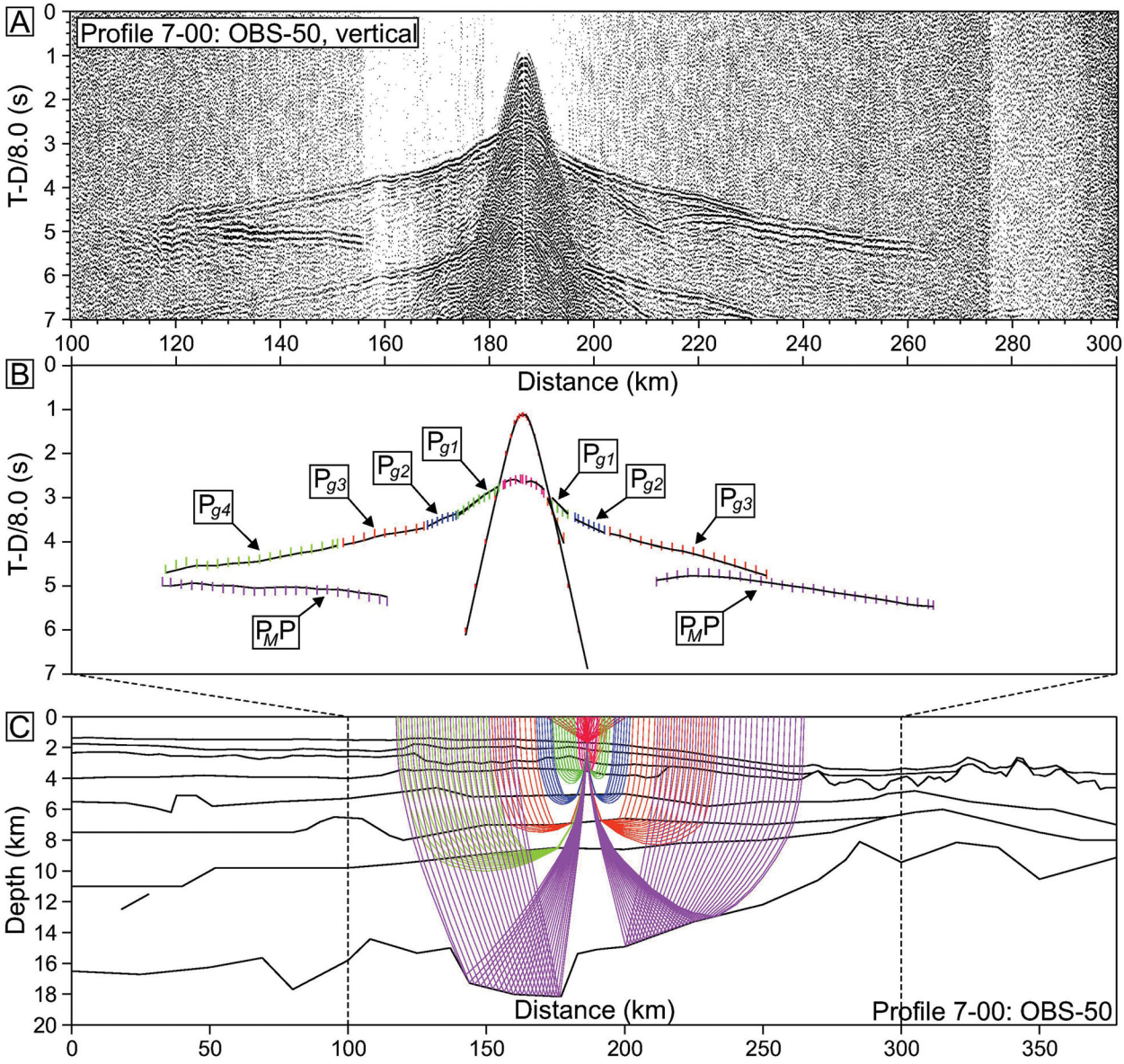

Figure 7. Data, interpretation and ray tracing of OBS 50, Profile 7-00, southern Jan Mayen microcontinent/Iceland Plateau. (A) OBS data, vertical component; (B) interpretation and model reproduction; and (C) ray tracing of the velocity model.

et al. 2012), but not the western side (Fig. 12D). Thus the existing magnetic data provide incomplete constraints on the development of the JMMC as it rifted from East Greenland. The JAS-05 aeromagnetic survey (Gernigon *et al.* 2009) is blended in with the older Verhoef *et al.* (1996) compilation in Fig. 12(D). The JAS-05 version shown here has a grid resolution of 2 × 2 km, upwards continued 2 km. It constrains the EJMFZ better than the gravity, so that the northern trace was moved up to 20 km northwards in the west, and ∼50 km closer to Jan Mayen, compared to the interpretation by Breivik *et al.* (2006).

Oceanic spreading on the Kolbeinsey Ridge resulted in clear magnetic seafloor spreading anomalies to the west. The Jan Mayen island and its surrounding areas have a strong, positive magnetic anomaly associated with recent volcanism. The JMR south of the island has a subdued magnetic field, and the magnetic quiet zone west of the ridge covers stretched continental crust (Kodaira *et al.* 1998). There are high-amplitude, positive anomalies in the Jan Mayen Trough. South of the trough, there is a linear, low-amplitude NNE trend. Talwani & Eldholm (1977) proposed that the pattern could be caused by continental fragments or ridges, embedded in oceanic crust. However, we do not find a clear correlation between the magnetic anomalies and the velocity structure (Fig. 9).

We use the magnetic tracks collected during seismic shooting to do a high-resolution study of the breakup process. Both tracks show the anomaly 24a/24b pair adjacent to the JMMC/Iceland Plateau (Figs 5 and 9), though they have a lower amplitude than on the Norwegian side. Anomaly identifications were tested through forward spreading rate modelling based on the timescale of Cande & Kent (1995), used to calculate synthetic magnetic anomalies (Figs 14 and 15). Past magnetic inclination and declination was set to equal that of the present Møre Margin, where the JMMC was at breakup time. Europe has also moved a few degrees to the north in relation to the

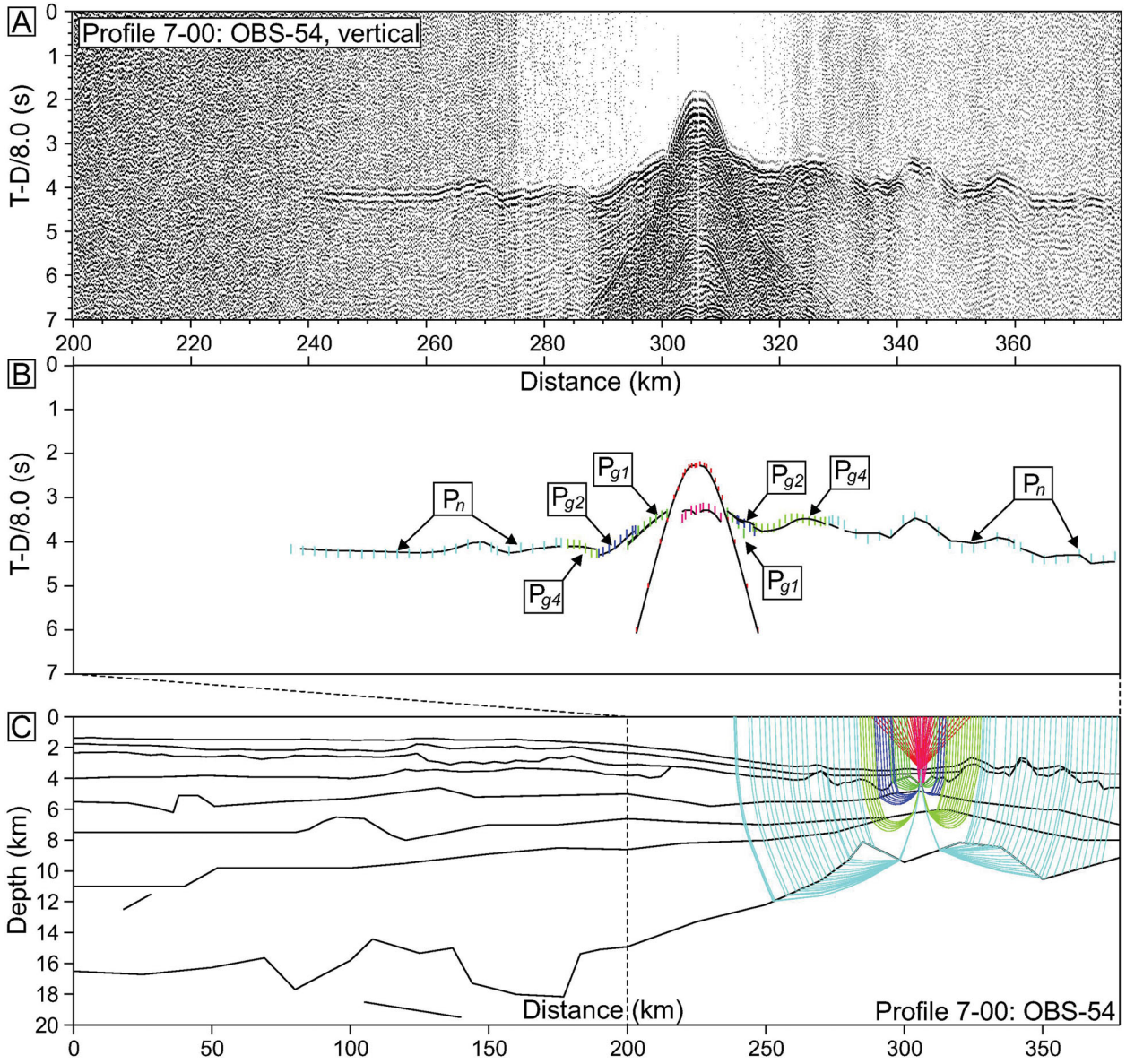

Figure 8. Data, interpretation and ray tracing of OBS 54, Profile 7-00, southern Jan Mayen microcontinent/Iceland Plateau–Norway Basin. (A) OBS data, vertical component. (B) Interpretation and model reproduction. (C) Ray tracing of the velocity model.

pole since then (e.g. Torsvik *et al.* 2001), which we have not tried to compensate for as the modelling results are insensitive to reasonable variations of these parameters. The spreading rates based on the forward magnetic modelling have an estimated uncertainty of ±2 mm a^{-1}. The profiles also need to be projected onto the spreading direction (Fig. 1). The estimated flowlines are from Breivik *et al.* (2006), which are strongly constrained by the EJMFZ. Additional uncertainty arises from the fairly high angle projection to spreading direction, and we show the effect of a 10° variation (Figs 14 and 15).

Profile 8-00 required a lower early opening rate than at the Norwegian side (Breivik *et al.* 2006 2009), but higher after anomaly 22 (Fig. 14D). This could be the result of asymmetric spreading or axial relocation. Profile 7-00 offers a complete section from crustal breakup to the extinction of spreading at the Aegir Ridge. After projection to the estimated spreading direction (Breivik *et al.* 2006), the spreading rates are comparable to that found at the eastern side of the Norway Basin, with early half-spreading rates exceeding 30 mm a^{-1}. The largest deviation occurs around anomaly 23, where rates are lower before, but higher afterwards. The transition to ultra-slow seafloor spreading occurs over anomaly 20, at ∼43 Ma (Cande & Kent 1995), as for the eastern side. This change was also detected around the EJMFZ from the JAS-05 magnetic data (Gernigon *et al.* 2009), but it does not occur at the Mohn Ridge to the north of the fracture zone (Mosar *et al.* 2002; Gernigon *et al.* 2009). The rapid fall in spreading rate is therefore likely to be caused by the onset of major stretching of the JMMC, then part of eastern Greenland. The slowest seafloor spreading recorded on both sides of the Aegir Ridge takes place during the following 3 Myr after this occurred. Seafloor spreading rates apparently increase somewhat after that, until the extinction of the Aegir Ridge at ∼25 Ma (Nunns 1982, 1983).

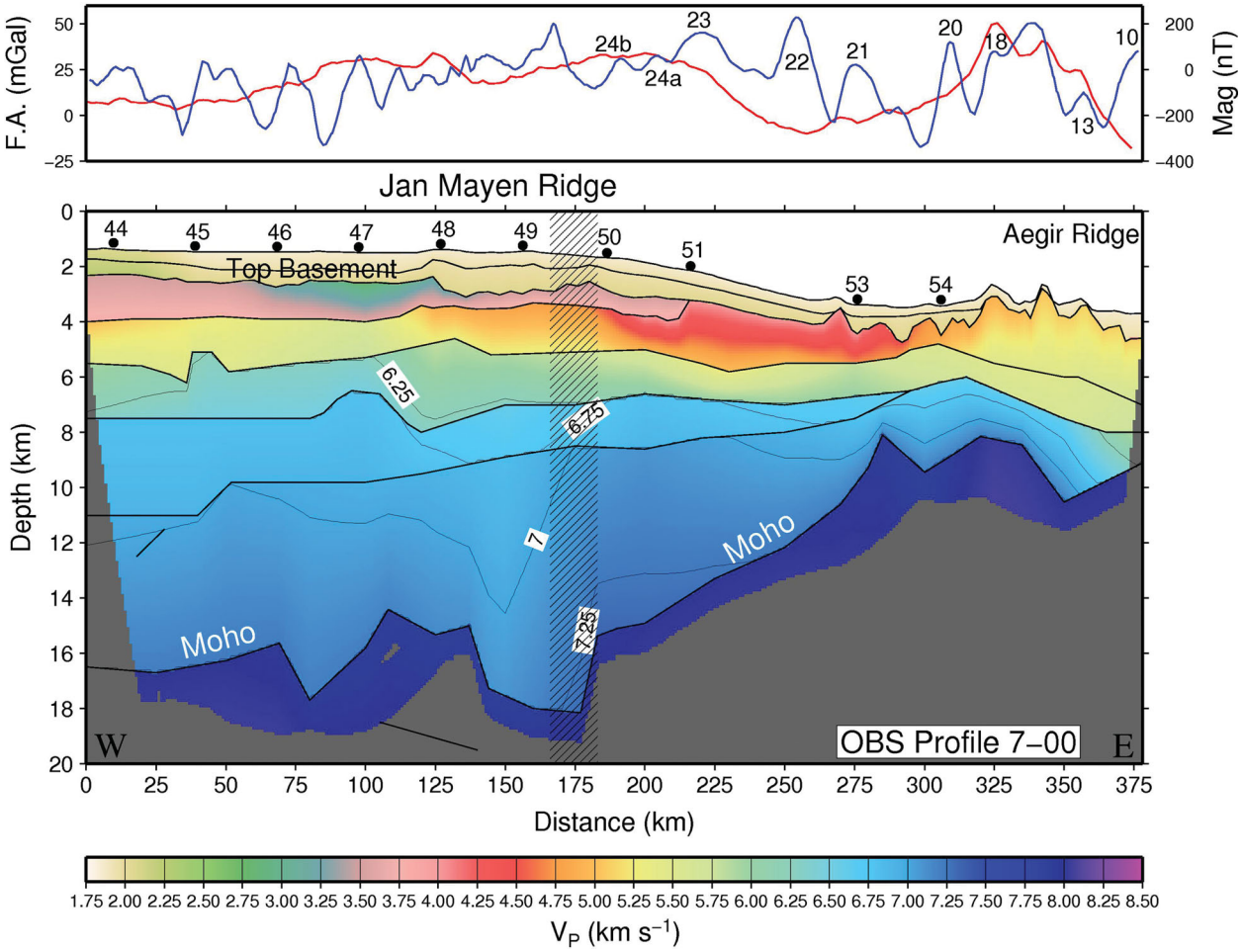

Figure 9. Gridded crustal velocity model for profile 7-00. The parts of the model not covered by *P*-wave rays are masked. Rays from floating reflectors do not constrain velocity and are not included in the ray coverage. The OBS locations are numbered on the seafloor. Hachure indicates the continent–ocean transition. Both gravity (red line) (Andersen *et al.* 2008) and magnetic anomalies (blue line) with anomaly identifications are shown in the panel above.

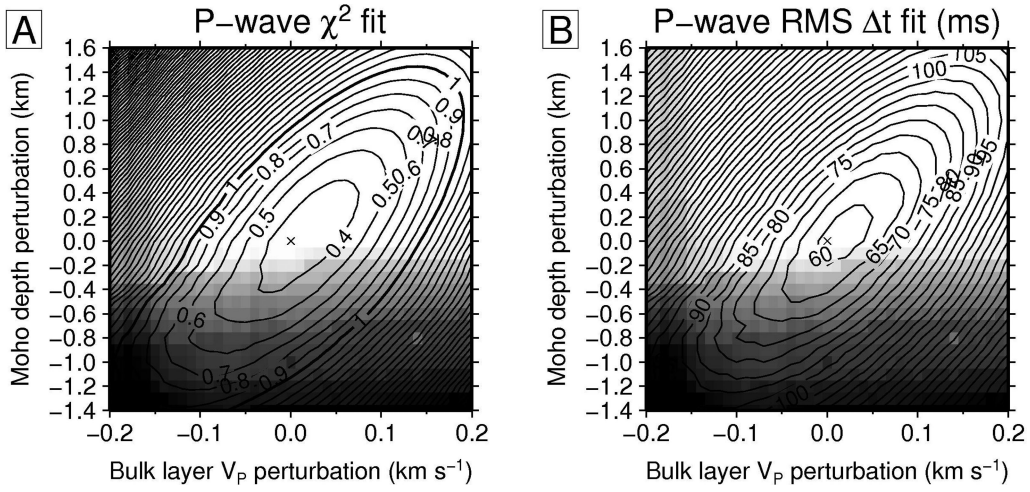

Figure 10. Profile 7-00 *P*-wave model sensitivity to lower crustal velocity changes against Moho depth between 180 and 280 km, based on P_{g4}, P_MP and P_n phases. Background shading indicates the ability of the model to trace arrivals to all observed locations. It starts at 2 per cent loss and reaches black at 15 per cent loss out of 413 picked arrivals. (A) *P*-wave χ^2 fit; (B) *P*-wave rms time fit.

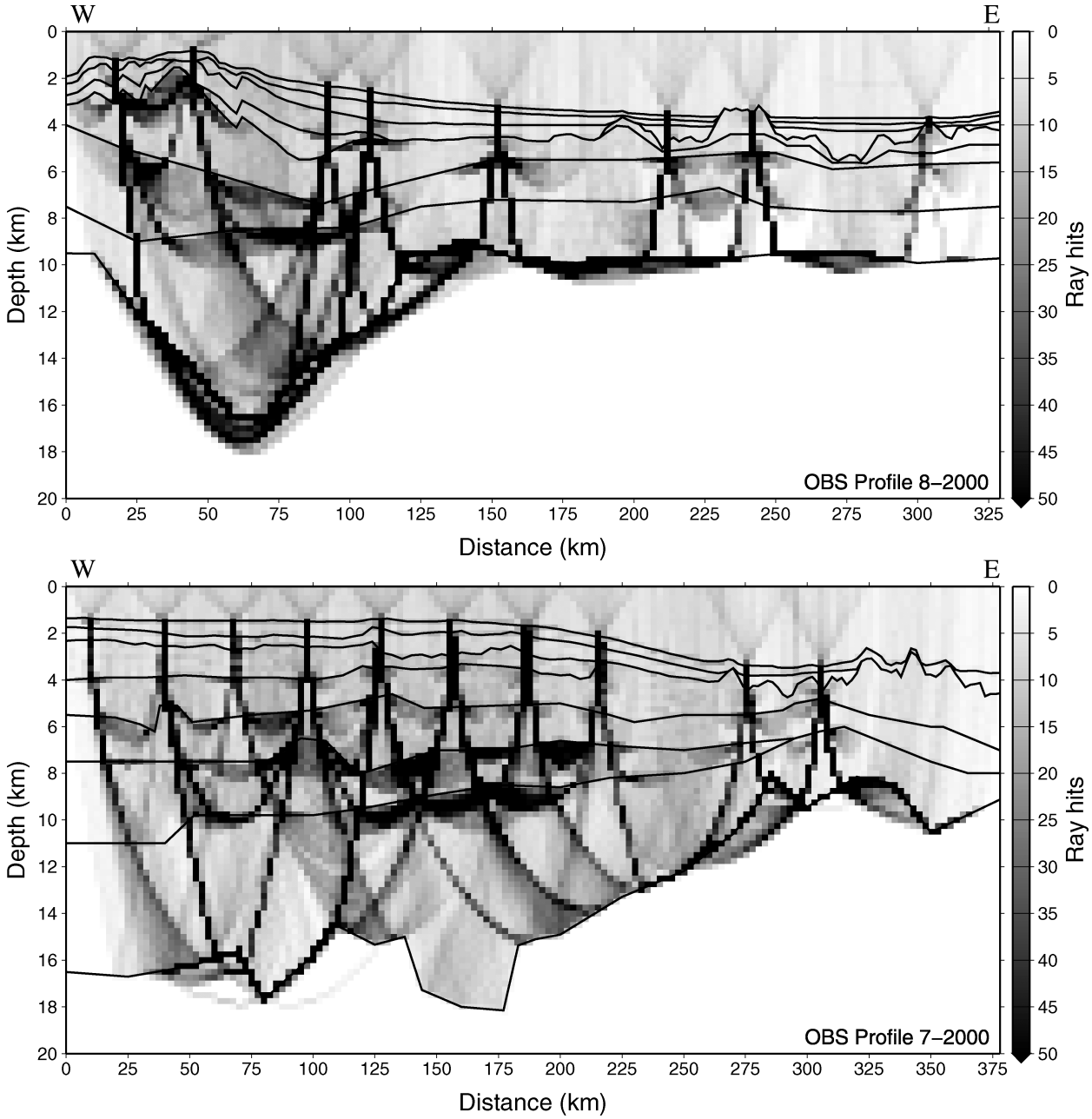

Figure 11. Ray hit count for 2.5 × 0.25 km grid cell size for Profile 7-00 and 8-00. Rays from floating reflectors do not constrain velocity and are not included.

5 DISCUSSION

The JMMC south of the Jan Mayen Trough has not previously been studied by deep seismic data, and the southern limit of the microcontinent is not easily identified (Talwani & Eldholm 1977). Before we take a closer look at the properties of the eastern volcanic margin on the profiles, we will shortly discuss the regional extent of both the JMMC and that of the breakup magmatism.

5.1 Microcontinent and volcanic margin extent

In addition to the OBS data, other data and plate tectonic considerations give good indications of the continental extent. The northern part must be limited by the EJMFZ, to fit in south of the Vøring Plateau (Fig. 12). Interpretation of the fracture zone system based on new magnetic data (Gernigon *et al.* 2009) constrains the EJMFZ south of the island of Jan Mayen. There are clear seafloor spreading anomalies up to anomaly 24 between the fracture zone traces (Gernigon *et al.* 2009). The JMMC must therefore extend to the northern fracture zone trace, but the island of Jan Mayen itself appears to be entirely volcanic. A recent plate reconstruction indicates the same (Gaina *et al.* 2009). It is therefore uncertain if there is a link between the southern EJMFZ trace and the northernmost fracture zone on the Kolbeinsey Ridge as proposed by Mjelde *et al.* (2008a). The northernmost part of the JMMC and of the eastern volcanic margin are poorly constrained, as are the offsets over the fracture zone. The latter are estimated from the magnetic anomaly pattern in the east, and by the offset of the fracture zone on the Kolbeinsey Ridge in the west (Fig. 12).

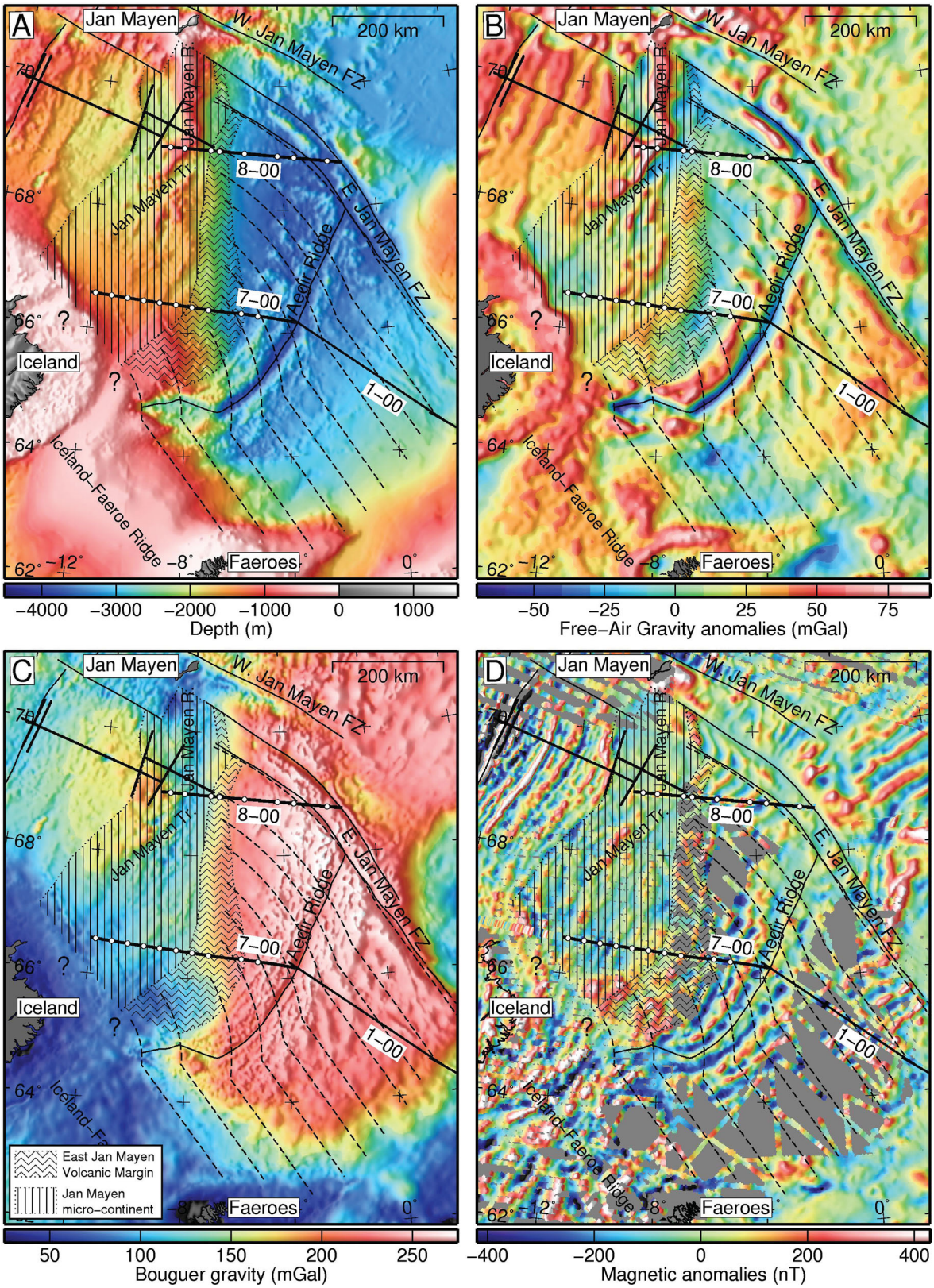

Figure 12. The extent of the Jan Mayen microcontinent and its eastern volcanic margin interpreted from OBS results and map data. All maps are illuminated from the west. Dashed lines represent estimated flowlines (Breivik *et al.* 2006). (A) Bathymetry (Jakobsson *et al.* 2008). (B) Free-air satellite-based gravity map (DNSC08) (Andersen *et al.* 2008). (C) Simple Bouguer map made from the satellite gravity map in B and from bathymetry in A. (D) Magnetic anomaly map over the study area (Verhoef *et al.* 1996), enhanced by the JAS-05 aeromagnetic survey in the north (Gernigon *et al.* 2009). Our year 2000 track data are also plotted along OBS lines.

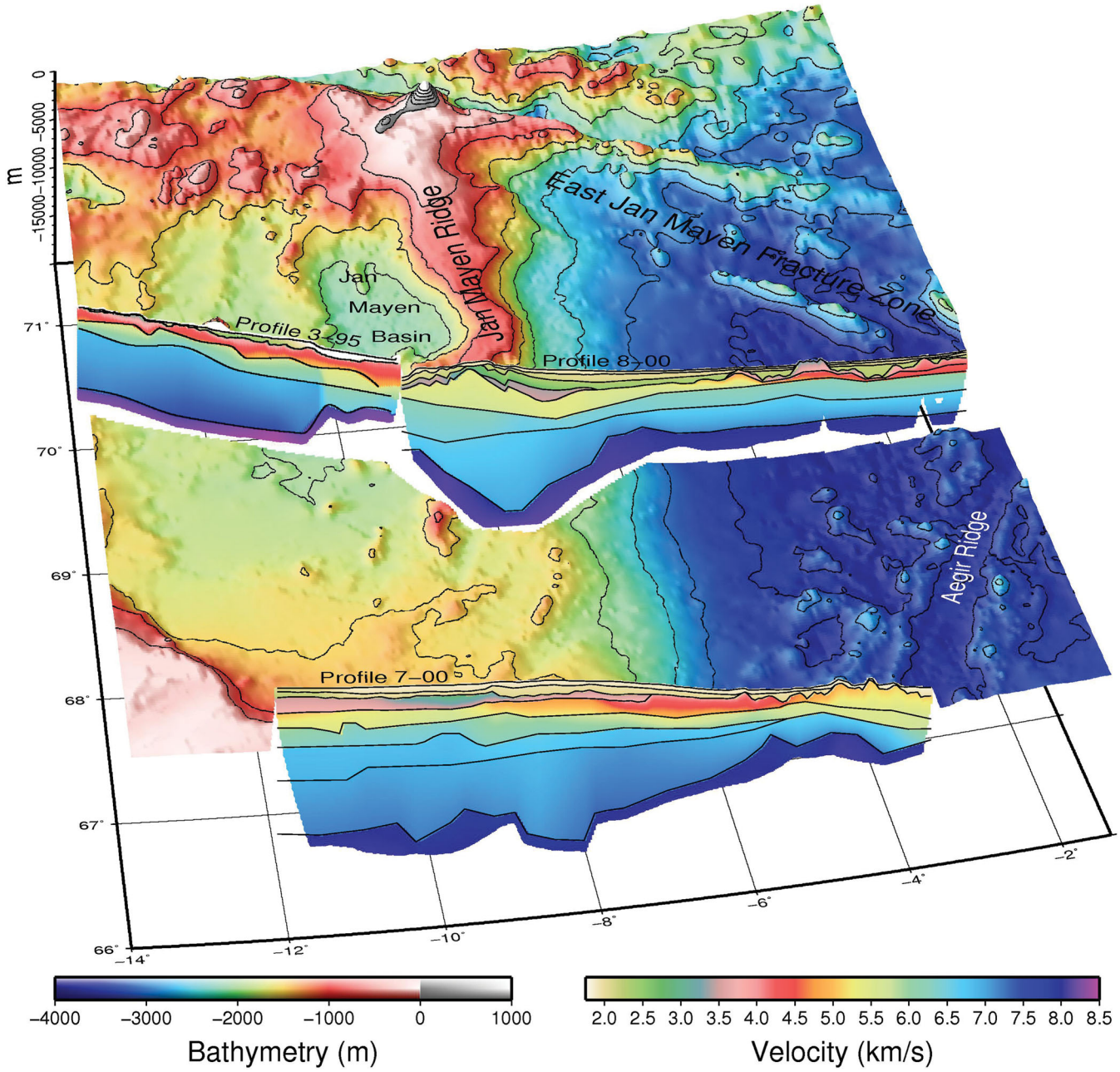

Figure 13. Perspective plot of Profiles 7-00 and 8-00 in a bathymetry cutout. The older Profile 3-95 is included to show the transition from the thin continental crust of the Jan Mayen Basin to the thick, high-velocity oceanic crust created at the Kolbeinsey Ridge to the west (Kodaira *et al.* 1997).

The western JMMC limit is well constrained by OBS data in the north (Kodaira *et al.* 1997, 1998) The old OBS Profile 3-95 is shown together with Profile 8-00 in a perspective plot of the bathymetry (Fig. 13). The seafloor of the models meets the seafloor grid at the cutout, following the shot line. The figure illustrates that the crust underlying the Jan Mayen Basin is both much thinner, and has lower velocity than the oceanic crust to the west, and that the transition from continental to oceanic crust takes place over a narrow zone. Note also the striking difference between the magma starved oceanic crust of the Norway Basin, and the thick oceanic crust of the Iceland Plateau. See Mjelde *et al.* (2008b) for a discussion of the complete crustal transect from the Norwegian to the East Greenland margins.

The continent–ocean transition obtained from Profile 3-95 in the northwest matches the appearance of the first magnetic seafloor spreading anomaly from the Kolbeinsey Ridge (Fig. 12D). These anomalies can be followed to the Iceland shelf in the SW, where they disappear into a chaotic pattern. If this defines the only seafloor spreading on the Iceland Plateau, that implies that the JMMC widens considerably to the south (e.g. Mjelde *et al.* 2008a), and that the western part of Profile 7-00 should be predominantly continental. However, an intermediate seafloor spreading axis west of the Aegir Ridge could have existed before seafloor spreading commenced at the Kolbeinsey Ridge (e.g. Vogt *et al.* 1970; Talwani & Eldholm 1977). However, this idea was later dismissed by Vogt *et al.* (1980), and as the data coverage has improved, there are still no obvious indications of any such seafloor spreading. Since the Aegir Ridge seafloor spreading slowed down at 42 Ma, plate movement must have been taken up elsewhere from then and up to 25 Ma when

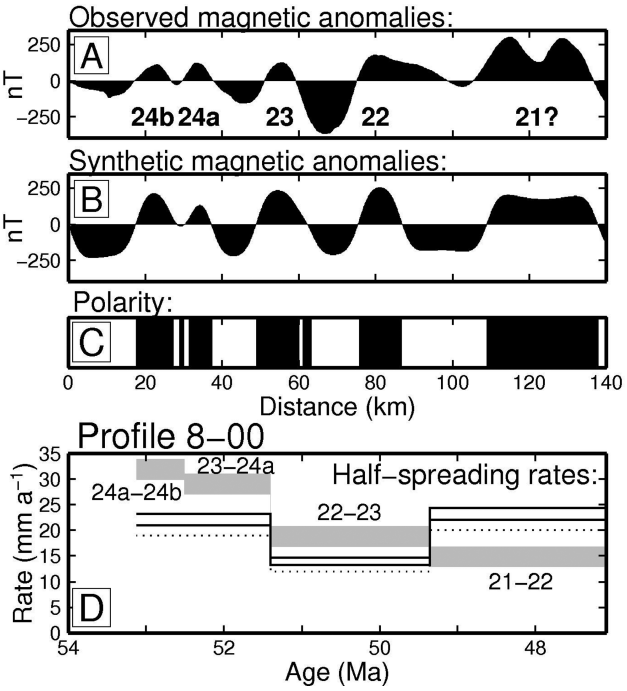

Figure 14. Magnetic anomalies along Profile 8-00. (A) Observed magnetic anomalies. Normal magnetic anomaly identifications are annotated in bold. (B) Synthetic magnetic anomalies calculated by an FFT routine from the spreading model, using a 4.5 km depth to the top of the 1-km-thick magnetized layer, and a magnetization of 4.2 A m^{-1} (Rabinowitz & LaBreque 1979). Magnetic inclination was set to 76.0°N, and magnetic declination to 6.2°W. (C) Polarity model versus distance calculated from (D). (D) Half-spreading rates. Dotted line is along profile, lower solid line is projected onto a spreading direction at a 25° angle, while the upper solid line is projected to a 35° angle. The grey-shaded line is from the eastern side of the Norway Basin (Breivik *et al.* 2006).

the Kolbeinsey Ridge spreading started. That there was a lot of extensional deformation of the JMMC in the north during breakup from East Greenland is well documented (e.g. Myhre *et al.* 1984; Gudlaugsson *et al.* 1988; Kodaira *et al.* 1998), and it is quite possible that this process would be sufficient to also account for the asymmetric seafloor spreading in the south (Nunns 1982; Skogseid & Eldholm 1987). Still, the JMMC is severely thinned in the northwest (Kodaira *et al.* 1998), while the crust in the south is both thicker, and has higher velocity (Figs 5, 9 and 13). As discussed above, the Bouguer gravity map (Fig. 12C) indicates that Profile 7-00 may be affected by igneous crustal growth near Iceland, which can explain these north to south differences.

The velocity is too high throughout the southern profile to give an unambiguous identification of continental crust, and we have to rely on more indirect arguments. The deepest Moho is located next to oceanic crust created during the earliest seafloor spreading in the Norway Basin, and the dimension is comparable to that of the JMMC on the northern profile (Fig. 13). The velocity falls slightly at mid-crustal levels here, and the gravity low above is slightly skewed to the west compared to the greatest Moho depth (Fig. 9), both indicating a different crustal composition compared to surrounding areas. An alternative interpretation could be that this region is the relic of an intermediate spreading ridge. There are two issues that speak against this. First of all, 18-km-thick oceanic crust must be produced during a period where the Iceland hotspot activity was low (e.g. White 1997). Later spreading on the Kolbeinsey Ridge produced only 9-km-thick oceanic crust during stronger hotspot activity (Kodaira *et al.* 1997). The interpretation would also imply that the Early Eocene volcanic margin was rifted off Greenland, leaving the continental crust behind. As the magnetic anomalies produce similar early plate spreading rates to that of the conjugate Møre Margin, the margin is clearly not affected by any igneous overprint from nearby later magmatism. Also the smooth tapering of the volcanic margin into the Norway Basin indicates that there was no later tectonic deformation. West of the volcanic margin, the magnetic field is subdued and comparable to that of continental crust to the north (Fig. 12D). Seafloor created around the Kolbeinsey Ridge shows linear, high-amplitude seafloor spreading anomalies. The Iceland-Faeroe Ridge and the Iceland shelf that were created through voluminous magmatism have similarly high magnetic amplitudes, but in a chaotic pattern. Taken together, these observations and considerations make us conclude that the JMMC is present in the western part of Profile 7-00 in the south, but also that it is probably affected by later magmatism tied to the growth of Iceland, which was also argued by Gaina *et al.* (2009). NNE-trending lower amplitude lineations seen around Profile 7-00 could indicate dyke intrusions of the JMMC south on the Iceland Plateau.

The continental crust may terminate at the proposed Faeroe Fracture Zone in the south, possibly linking the continental Clair lineament to the Tjörnes Fracture Zone in northernmost Iceland (e.g. Kimbell *et al.* 2005; Mjelde *et al.* 2008a). There was an offset between the Aegir and Reykjanes ridges, but the link between the two is obscured by the extensive magmatism of the Iceland-Faeroe Ridge. Zircons of Mesozoic age found in NE Iceland indicate that continental crust may be present SW of the proposed lineament (Paquette *et al.* 2006).

Similar to that of the conjugate Møre-Faeroes margin (Berndt *et al.* 2001; Breivik *et al.* 2006; White *et al.* 2008), there is a north to south increase in magma productivity. The width of the thickened oceanic crust of the volcanic margin increases greatly from north to south (Fig. 12). Breakup magmatism was over by ∼52.5 Ma at Profile 8-00, by ∼51.5 Ma on Profile 1-00 on the conjugate margin slightly to the south (Breivik *et al.* 2006) and by ∼47 Ma on Profile 7-00. The duration of excess magmatism at Profile 8-00 in the north may be as short as 1–1.5 Myr (Fig. 5), while at Profile 7-00 in the south excess magmatism was greater and lasted up to ∼7 Myr (Figs 9 and 14). The part of the volcanic margin extrapolated to the south past Profile 7-00 probably curves more to the west than that proposed by Mjelde *et al.* (2008a), as indicated by the synthetic flowlines backcalculated from the Aegir Ridge (Breivik *et al.* 2006).

5.2 Igneous thickness compared to velocity (H-V_P)

Seafloor spreading causes passive, corner-flow mantle upwelling underneath the spreading axis, and as mantle rocks cross the solidus the mantle undergoes partial melting. The more incompatible elements enter the melt phase first, and different minerals melt at different degrees of melting over different pressure ranges (e.g. Klein & Langmuir 1987; McKenzie & Bickle 1988). Increasing the melt degree will give an increased MgO content, resulting in higher velocity of the igneous rocks (e.g. White 1989; Korenaga *et al.* 2002). Elevated temperature will increase the mantle melt degree, and therefore give a positive correlation between velocity and thickness of the igneous section produced at volcanic margins. Other mechanisms that could govern magma productivity will give different correlations. Active mantle convection giving increased

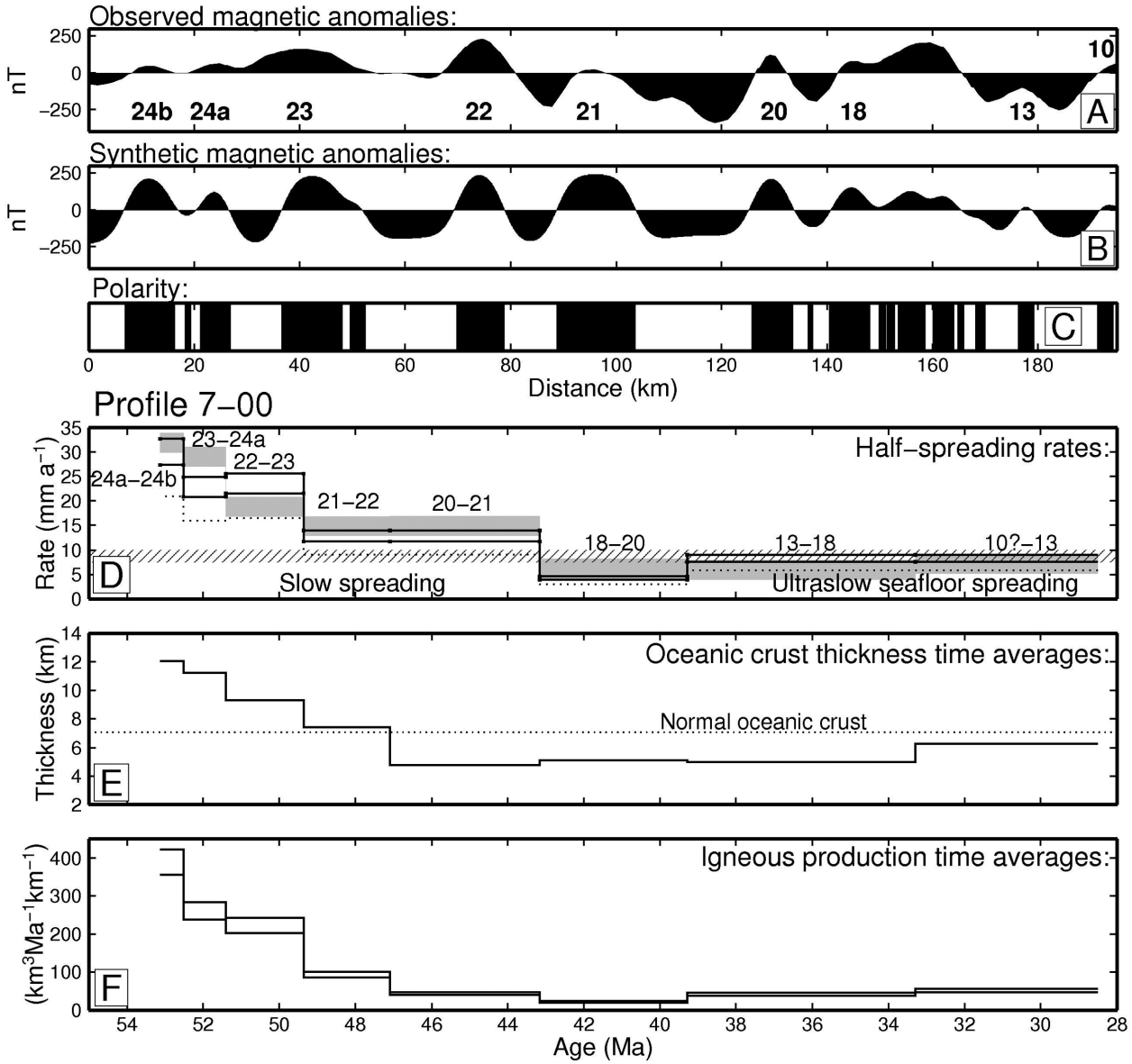

Figure 15. Magnetic anomalies along Profile 7-00. (A) Observed magnetic anomalies. Normal magnetic anomaly identifications are annotated in bold. (B) Synthetic magnetic anomalies, applying the parameters in Fig. 14. (C) Polarity model versus distance calculated from (D). (D) Half-spreading rates. Dotted line is along profile, lower solid line is projected onto a spreading direction at a 40° angle, while the upper solid line is projected to a 50° angle. The broad, grey-shaded line is from the eastern side of the Norway Basin (Breivik *et al.* 2006). The transition from slow to ultraslow seafloor spreading is indicated by hachure (E) Oceanic crustal thickness time averages between magnetic anomalies. (F) Igneous production half-rate time averages computed from (D) and (E), using the two different spreading direction projections.

flux of mantle material through the melt zone will produce thicker igneous crust at a lower melt degree (Holbrook *et al.* 2001; Parkin & White 2008), which will result in low correlation. If the mantle melting is controlled by enriched mantle components, the result will be a negative correlation (Korenaga *et al.* 2002; Sallarès *et al.* 2005; Parkin & White 2008).

Magma fractionation in the crust will enrich minerals with high velocity in the lower crust, which would bias the analysis. On the other hand, fractionation in the upper mantle will prevent these components from becoming part of the crust, and would lower crustal velocity. It is believed that these processes may cancel each other (e.g. Korenaga *et al.* 2002; Parkin & White 2008), and that the main problem with finding a mean velocity of the igneous section is tied to the effect of cracks and fissures, which lower the velocity. This effect dominates the upper oceanic crust (Wilkens *et al.* 1991; Jacobson 1992), and must be corrected for. Also, velocities are both pressure and temperature dependent (e.g. Fountain & Christensen 1989). To make results and melting models comparable, velocities should also be corrected from the *in situ* temperature and pressure to a reference state. To estimate the *in situ* conditions, we use 0.00022 km s^{-1} MPa^{-1} and −0.0005 km s^{-1} $°C^{-1}$ (Holbrook *et al.* 2001), assuming a linear temperature gradient from 10 °C at the seafloor to 750 °C at 40 km depth. Corrections are applied to each grid cell of the gridded velocity models (Figs 5 and 9), before calculating the mean velocity. Pressure is estimated by first converting velocity to density following the empirical relationship of Ludwig

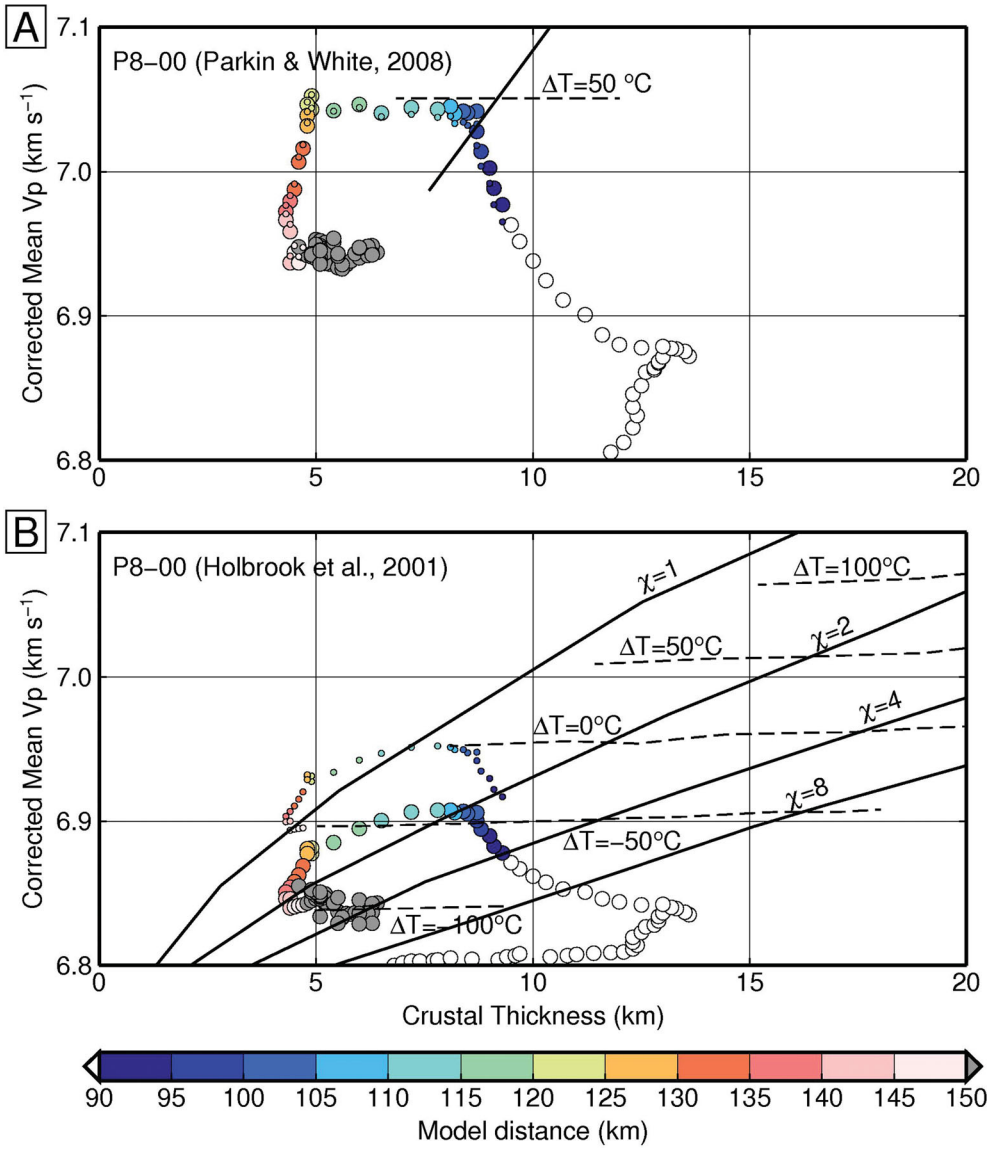

Figure 16. Crustal thickness variations plotted against mean V_P for the igneous crust for Profile 8-00. Large circles are pressure and temperature corrected, while small circles are uncorrected. The colour coding indicates the profile positions for the data, where grey symbols indicate thin oceanic crust, and white symbols the continental ridge and westwards. (A) Using the Parkin & White (2008) and White *et al.* (2008) approach. The reference curve for mantle melting is based on Sallarès *et al.* (2005), as presented by White *et al.* (2008). The temperature increase over normal seafloor spreading to produce a given velocity is from White *et al.* (2008). (B) Mean crustal velocity based on the corrections of Holbrook *et al.* (2001). The mantle melting lines are from the same source, where χ indicates the degree of active upwelling ($\chi = 1$ is passive). Mantle temperature anomalies are relative to 1300 °C.

et al. (1970). The weight of the overlying column, including the seawater, can then be calculated.

Different corrections have been used by different authors, so that the mean velocity cannot necessarily be directly compared between studies, but only to their own reference models. To reduce the effect of porosity, Holbrook *et al.* (2001) adjusted upper crustal velocities lower than 6.85 km s^{-1} up to that value, before temperature and pressure correction to 400 °C and 600 MPa. Parkin & White (2008) and White *et al.* (2008) ignored the upper crust altogether in the velocity calculations, and only used the lower crust having a velocity above 6.7 km s^{-1}. They further used a reference temperature of 150 °C and a pressure of 230 MPa, which is typical for the lower crustal conditions of the NE Atlantic margins. Their velocity data were therefore not corrected before calculating velocity means. We tried out both of these procedures on our profiles. Also the effect of actually doing pressure and temperature corrections for the Parkin & White (2008) procedure was tested, and proves to be minor. On the other hand, the effects are major for the Holbrook *et al.* (2001) procedure.

We take a closer look at the properties of the volcanic margin of the eastern JMMC, starting in the north. Using the corrections of Holbrook *et al.* (2001), the mean velocity shows a positive correlation with crustal thickness here, indicating a 50 °C temperature drop from breakup to normal seafloor spreading (Fig. 16B). However, the velocity curve is low in the diagram, indicating a drop from a −50 °C to −100 °C temperature anomaly relative to a normal 1300 °C mantle temperature. The result is curious in that it indicates an elevated temperature at breakup, but within an

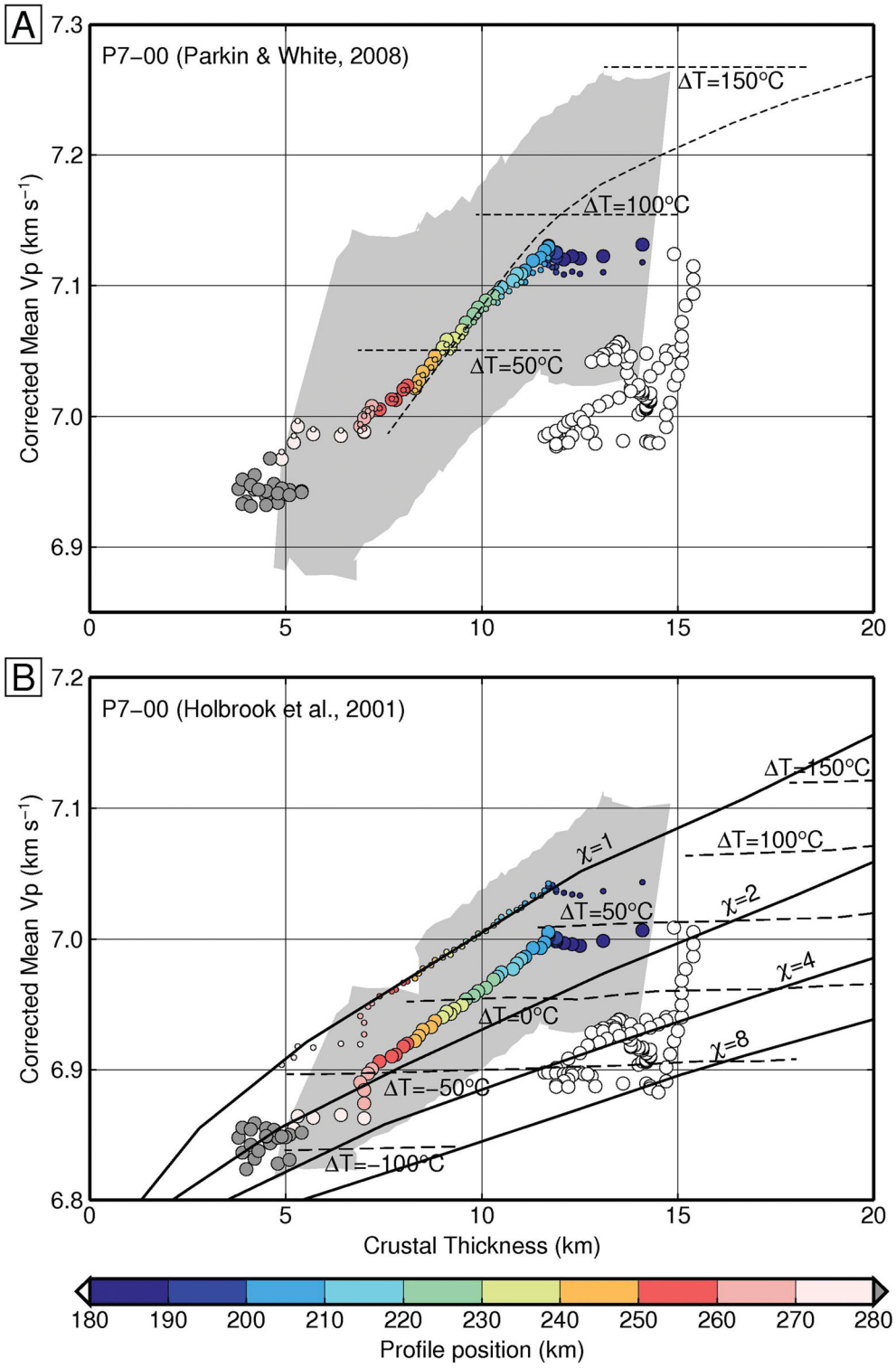

Figure 17. Crustal thickness variations plotted against mean V_P for Profile 7-00. See Fig. 16 for details. The grey shading indicates the model uncertainty derived from Fig. 10. (A) Using the corrections of Parkin & White (2008) and White *et al.* (2008). (B) Mean crustal velocity based on the corrections of Holbrook *et al.* (2001).

unusually cold mantle. On the other hand, using the procedure of Parkin & White (2008), the mean velocity is higher, but the curve shape has changed (Fig. 16A). Since only the lower crust is used in the calculations, the results are more sensitive to the variations there with this procedure. However, the velocities of the thin oceanic crust indicate normal mantle temperature. Both models indicate a 50 °C mantle temperature drop from breakup to normal seafloor spreading.

Profile 7-00 shows that an oceanic crust up to 12 km thick was produced after breakup (Fig. 9). Both correction procedures give a positive H-V_P correlation from 4 to 12 km thickness (Fig. 17). In the Holbrook *et al.* (2001) diagram, the data points lie between passive

and two-times active upwelling, but with passive upwelling within the estimated uncertainty (Fig. 10). The predicted initial positive mantle temperature anomaly is ∼50 °C, followed by a temperature drop of as much as 150 °C. Using the procedure of Parkin & White (2008), the temperature anomaly at breakup becomes ∼90 °C. This is higher than that obtained by using Holbrook *et al.* (2001), but the cooling trend is at ∼90 °C less (Fig. 17).

The H-V_P correlation is positive from the Norway Basin up to 200 km in the model (Fig. 9). From there the level flattens out to 175 km, and west of that the velocity falls over what we interpret to be the southern JMMC. The mean velocities do not reach the same high levels farther west, indicating older continental crust mixed with Cenzoic igneous rocks, consistent with the plate tectonic considerations above.

6 SUMMARY AND CONCLUSIONS

Two OBS profiles were acquired across the northern and southern JMMC/Iceland Plateau, respectively, both extending into the oceanic western Norway Basin. The data were modelled by ray tracing of the *P* waves, giving velocity transects of the crust and uppermost mantle. The eastern JMMC margin is conjugate to the passive volcanic Møre-Faeroes Margin.

The Early Eocene breakup magmatism was moderate in the north, and the continental part is easily identified. Both profiles show a maximum Moho depth of 17–18 km under the eastern JMMC/Iceland Plateau. Late Oligocene breakup from Greenland extended the northwestern JMMC down to a thickness of 5–7 km (Kodaira *et al.* 1998). However, at the southern profile the crust is 14–17 km thick under the Iceland Plateau. The magnetic map does not show clear seafloor spreading anomalies here, and the magnetic anomaly amplitudes are lower than in the adjacent oceanic basins. Our preferred interpretation is therefore that the area consists of older continental crust with a newer magmatic addition. Being close to Iceland, this could be caused by the Iceland hotspot throughout continental rifting, or by post-rift magmatic growth of the crust due to the Neogene emergence of Iceland nearby. The volcanic margin itself shows every characteristic of the conjugate margin, and appears unaffected by tectonism or by secondary magmatism since breakup.

Our magnetic track data show seafloor spreading rates off the southeastern JMMC comparable to that of the conjugate Møre Margin (Breivik *et al.* 2006). Both sides show the transition from slow to ultraslow seafloor spreading to occur at ∼43 Ma. We interpret this as the response to the onset of major stretching of the western JMMC at that time, which would take up some of the movement between Europe and Greenland.

The Early Eocene breakup magmatism increased from north to south. It lasted 1–1.5 Myr and produced up to ∼3 km of extra crustal thickness compared to the later seafloor spreading in the north. At the southern profile, the early igneous section is ∼8 km thicker, and excess magmatism lasted up to ∼7 Myr. Igneous thickness has a positive correlation with corrected mean *P*-wave velocity. This is consistent with excess magmatism being caused by elevated mantle temperature, and there is no evidence of small-scale mantle convection or increased mantle melt fertility contributing. We tried two related, but slightly different procedures to estimate the mantle temperature anomaly. Using the Parkin & White (2008) procedure, the excess mantle temperature is estimated to ∼90 °C in the south. By using the procedure of Holbrook *et al.* (2001) it is estimated to as much as ∼150 °C. Both procedures estimate the temperature anomaly to ∼50 °C in the north. Absolute mantle temperature estimates differ between the two, but the trend should be more robust in diagnosing process rather than the absolute level of the velocity, and here they agree.

ACKNOWLEDGMENTS

The crew of R/V Håkon Mosby and engineers from the University of Bergen are greatly acknowledged for their skills and help. We also thank H. Shimamura, T. Yamashina and T. Watanabe from Hokkaido University for invaluable participation in planning and executing the survey. The Norwegian Petroleum Directorate (NPD) and Norsk Hydro initiated and funded this project, with thanks in particular to E. Bråstein and H. Brekke (NPD) and R. Karpuz (Norsk Hydro, now Statoil). We also thank Bryndís Brandsdóttir for many discussions during development of the manuscript. Comments from Laurent Gernigon and an anonymous reviewer, and from the editor Saskia Goes, greatly helped to improve the manuscript for publication. The modelling was done using the Rayinvr modelling software developed by C. Zelt (Rice University, Houston). Maps and some figures were prepared with the GMT program package (Wessel & Smith 1991, 1998), and the seismic processing was performed by Seismic Unix tools (http://www.cwp.mines.edu/cwpcodes/). Finally, we would like to thank NGU (the Norwegian Geological Survey) and L. Gernigon for access to the JAS-05 aeromagnetic survey.

REFERENCES

Andersen, O.B. & Knudsen, P., 2009. DNSC08 mean surface and mean dynamic topography models, *J. geophys. Res.,* **114,** (C11001), doi:10.1029/2008JC005179.

Andersen, O.B., Knudsen, P., Berry, P. & Kenyon, S., 2008. The DNSC08 ocean wide altimetry derived gravity field, *Geophys. Res. Abstr.,* **10,** EGU2008-A-07163.

Berndt, C., Planke, S., Alvestad, E., Tsikalas, F. & Rasmussen, T., 2001. Seismic volcanostratigraphy of the Norwegian Margin: constraints on tectonomagmatic break-up processes, *J. geol. Soc.,* **158,** 413–426.

Brandsdóttir, B., Hooft, E.E.E., Breivik, A.J., Mjelde, R., Shimamura, H., & Murai, Y., 2008. Origin and evolution of the Iceland Plateau, *EOS, Trans. Am. geophys. Un.,* **89**(53), Fall Meet. Suppl., Abstract T12D-0492.

Breivik, A.J., Mjelde, R., Faleide, J.I. & Murai, Y., 2006. Rates of continental breakup magmatism and seafloor spreading in the Norway Basin–Iceland plume interaction, *J. geophys. Res.,* **111,** B07102, doi:10.1029/2005JB004004.

Breivik, A.J., Faleide, J.I., Mjelde, R. & Flueh, R., 2009. Magma productivity and early seafloor spreading rate correlation on the northern Vøring Margin, Norway: constraints on mantle melting, *Tectonophysics,* **468,** 206–223.

Cande, S.C. & Kent, D.V., 1995. Revised calibration of the geomagnetic polarity time scale for Late Cretaceous and Cenozoic, *J. geophys. Res.,* **100**(B4), 6093–6095.

Dick, H.J.B., Lin, J. & Schouten, H., 2003. An ultraslow-spreading class of ocean ridge, *Nature,* **426,** 405–411.

Fountain, D.M. & Christensen, N.I., 1989. Composition of the continental crust and upper mantle: a review, in *Geophysical Framework of the Continental United States,* Vol. 172, pp. 711–742, eds Pakiser, L.C. & Mooney, W.D., Geological Society of America, Boulder, CO.

Gaina, C., Gernigon, L. & Ball, P., 2009. Palaeocene: recent plate boundaries in the NE Atlantic and the formation of the Jan Mayen microcontinent, *J. geol. Soc.,* **166,** 601–616.

Gernigon, L., Olesen, O., Ebbing, J., Wienecke, S., Gaina, C., Mogaard, J.O., Sand, M. & Myklebust, R., 2009. Geophysical insights and early spreading history in the vicinity of the Jan Mayen Fracture Zone, Norwegian–Greenland Sea, *Tectonophysics,* **468,** 185–205.

Gernigon, L., Gaina, C., Olesen, O., Ball, P.J., Péron-Pinvidic, G. & Yamasaki, T., 2012. The Norway Basin revisited: from continental breakup to spreading ridge extinction, *Mar. Petrol. Geol.,* in press.

Greenhalgh, E.E. & Kusznir, N.J., 2007. Evidence for thin oceanic crust on the extinct Aegir Ridge, Norwegian Basin, NE Atlantic derived from satellite gravity inversion, *Geophys. Res. Lett.,* **34,** L06305, doi:10.1029/2007GL029440.

Gudlaugsson, S.T., Gunnarson, K., Sand, M. & Skogseid, J., 1988. Tectonic and volcanic events at the Jan Mayen Ridge microcontinent, in *Early Tertiary Volcanism and the Opening of the NE Atlantic,* Vol. 39, pp. 85–93, eds Morton, A.C. & Parson, L.M., Geol. Soc. Spec. Publ., London.

Holbrook, W.S. *et al.*, 2001. Mantle thermal structure and active upwelling during continental breakup in the North Atlantic, *Earth planet. Sci. Lett.,* **190,** 251–266.

Jacobson, R.S., 1992. Impact of crustal evolution on changes of the seismic properties of the uppermost oceanic crust, *Rev. Geophys.,* **30**(1), 23–42.

Jakobsson, M., Macnab, R., Mayer, L., Anderson, R., Edwards, M., Hatzky, J., Schenke, H.W. & Johnson, P., 2008. An improved bathymetric portrayal of the Arctic Ocean: Implications for ocean modeling and geological, geophysical and oceanographic analyses, *Geophys. Res. Lett.,* **35,** L07602, doi:10.1029/2008GL033520.

Kimbell, G.S., Ritchie, J.D., Johnson, H. & Gatliff, R.W., 2005. Controls on the structure and evolution of the NE Atlantic margin revealed by regional potential field imaging and 3D modelling, in *Petroleum Geology: North-West Europe and Global Perspectives Proceedings of the 6th Petroleum Geology Conference,* pp. 933–945, eds Doré, A.G. & Vining, B.A., Geological Society, London.

Klein, E.M. & Langmuir, C.H., 1987. Global correlations of ocean ridge basalt chemistry with axial depth and crustal thickness, *J. geophys. Res.,* **92**(B8), 8089–8115.

Kodaira, S., Mjelde, R., Shimamura, H., Gunnarsson, K. & Shiobara, H., 1997. Crustal structure of the Kolbeinsey Ridge, N. Atlantic, obtained by use of Ocean Bottom Seismographs, *J. geophys. Res.,* **102**(B2), 3131–3151.

Kodaira, S., Mjelde, R., Gunnarsson, K., Shiobara, H. & Shimamura, H., 1998. Structure of the Jan Mayen microcontinent and implication for its evolution, *Geophys. J. Int.,* **132,** 383–400.

Korenaga, J., Kelemen, P.B. & Holbrook, W.S., 2002. Methods for resolving the origin of large igneous provinces from crustal seismology, *J. geophys. Res.,* **107**(B9), 2178, doi:10.1029/2001JB001030.

Kuvaas, B. & Kodaira, S., 1997. The formation of the Jan Mayen microcontinent: the missing piece in the continental puzzle between the Møre-Vøring Basins and East Greenland, *First Break,* **15,** 239–247.

Ludwig, W.I., Nafe, J.E. & Drake, C.L., 1970. Seismic refraction, *The Sea,* **4**(1), 53–84.

Lundin, E. & Doré, A.G., 2002. Mid-Cenozoic post-breakup deformation in the passive margins bordering the Norwegian–Greenland Sea, *Mar. Petrol. Geol.,* **19,** 79–93.

Malinverno, A., 1991. Inverse square-root dependence of mid-ocean-ridge flank roughness on spreading rate, *Nature,* **352,** 58–60.

McKenzie, D. & Bickle, M.J., 1988. The volume and composition of melt generated by extension of the lithosphere, *J. Petrol.,* **29**(3), 625–679.

Mjelde, R., Raum, T., Myhren, B., Shimamura, H., Murai, Y., Takanami, T., Karpuz, R. & Næss, U., 2005. Continent-ocean transition on the Vøring Plateau, NE Atlantic, derived from densely sampled ocean bottom seismometer data, *J. geophys. Res.,* **110**, doi:10.1029/2004JB003026.

Mjelde, R., Eckhoff, I., Solbakken, S., Kodaira, S., Shimamura, H., Gunnarsson, K., Nakanishi, A. & Shiobara, H., 2007. Gravity and S-wave modeling across the Jan Mayen Ridge, North Atlantic: implications for crustal lithology and continental break-up processes, *Mar. geophys. Res.,* **28,** 27–41.

Mjelde, R., Breivik, A.J., Raum, T., Mittelstaedt, E., Ito, G. & Faleide, J.I., 2008a. Magmatic and tectonic evolution of the North Atlantic, *J. geol. Soc.,* **165,** 31–42.

Mjelde, R., Raum, T., Breivik, A.J. & Faleide, J.I., 2008b. Crustal transect across the North Atlantic, *Mar. geophys. Res.,* **29,** 73–87.

Mosar, J., Lewis, G. & Torsvik, T.H., 2002. North Atlantic sea-floor spreading rates: implications of the Tertiary development of inversion structures of the Norwegian-Greenland Sea, *J. geol. Soc.,* **159,** 503–515.

Myhre, A.M., Eldholm, O. & Sundvor, E., 1984. The Jan Mayen Ridge: present status, *Polar Res.,* **2,** 47–59.

Nunns, A., 1982. The structure and evolution of the Jan Mayen Ridge and surrounding regions, in *Studies in Continental Margin Geology,* Vol. 34, pp. 193–208, eds Watkins, J.S. & Drake, C.L., American Association of Petroleum Geologists, Tulsa, OK.

Nunns, A.G., 1983. Plate tectonic evolution of the Greenland- Scotland Ridge and surrounding regions, in *Structure and Development of the Greenland-Scotland Ridge: New Methods and Concepts,* pp. 11–30, eds Bott, M.H.P., Saxow, S., Talwani, M. & Thiede, J., NATO Advanced Research Institute/Plenum Press, New York, NY.

Olesen, O. *et al.*, 2010. *Magnetic Anomaly Map, Norway and Adjacent Areas, 1:3 million,* Geological Survey of Norway, Trondheim.

Paquette, J., Sigmarsson, O. & Tiepolo, M., 2006. Continental basement under Iceland revealed by old zircons., *EOS, Trans. Am. Geophys. Un.,* **87,** Fall Meet. Suppl., Abstract V33A–0642.

Parkin, C.J. & White, R.S., 2008. Influence of the Iceland mantle plume on oceanic crust generation in the North Atlantic, *Geophys. J. Int.,* **173,** 168–188.

Parkin, C.J., Lunnon, Z.C., White, R.S., Christie, P.A.F. & iSIMM Team, 2007. Imaging the pulsing Iceland mantle plume through the Eocene, *Geology,* **35**(1), 93–96.

Planke, S., 1994. Geophysical response of flood basalts from analysis of wire line logs: Ocean Drilling Program Site 642, Vøring volcanic margin, *J. geophys. Res.,* **99,** 9279–9296.

Rabinowitz, P.D. & LaBreque, J., 1979. The Mesozoic south Atlantic ocean and evolution of its continental margins, *J. geophys. Res.,* **84**(B11), 5973–6002.

Sallarès, V., Charvis, P., Flueh, E.R., Bialas, J. & the SALIERI Scientific Party, 2005. Seismic structure of the Carnegie ridge and the nature of the Galápagos hotspot, *Geophys. J. Int.,* **161,** 763–788.

Skogseid, J. & Eldholm, O., 1987. Early Cenozoic crust at the Norwegian continental margin and the conjugate Jan Mayen Ridge, *J. geophys. Res.,* **92**(B11), 11 471–11 491.

Talwani, M. & Eldholm, O., 1977. Evolution of the Norwegian–Greenland Sea, *Geol. Soc. Am. Bull.,* **88,** 969–999.

Torsvik, T.H., Van der Voo, R., Meert, J.G., Mosar, J. & Walderhaug, H.J., 2001. Reconstructions of the continents around the North Atlantic at about the 60th parallel, *Earth Planet. Sci. Lett.,* **187,** 55–69.

Verhoef, J., *et al.*, 1996. *Magnetic Anomalies of the Arctic and North Atlantic Oceans and Adjacent Land Areas,* Technical Report, Geol. Surv. Canada, Dartmouth.

Vogt, P.R., Ostenso, N.A. & Johnson, G.L., 1970. Magnetic and bathymetric data bearing on sea-floor spreading north of Iceland, *J. geophys. Res.,* **75**(5), 903–920.

Vogt, P.R., Johnson, G.L. & Kristjansson, L., 1980. Morphology and magnetic anomalies north of Iceland, *J. Geophys.,* **47,** 67–80.

Wessel, P. & Smith, W.H.F., 1991. Free software helps map and display data, *EOS, Trans. Am. geophys. Un.,* **72**(441), 445–446.

Wessel, P. & Smith, W.H.F., 1998. New, improved version of Generic Mapping Tools released, *EOS, Trans. Am. geophys. Un.,* **79,** 579.

White, R.S., 1989. Initiation of the Iceland Plume and opening of the North Atlantic, in *Extensional Tectonics and Stratigraphy of the North Atlantic Margins,* AAPG Mem. 46, pp. 149–154, eds Tankard, A.J. & Balkwill, H.R., American Association of Petroleum Geologists, Tulsa, OK.

White, R.S., 1997. Rift-plume interaction in the North Atlantic, *Phil. Trans. R. Soc. Lond.,* **355**(1723), 319–339.

White, R.S., McKenzie, D. & O'Nions, K., 1992. Oceanic crustal thickness from seismic measurements and rare earth element inversion, *J. geophys. Res.,* **97**(B13), 19 683–19 715.

White, R.S., Smith, L.K., Roberts, A.W., Christie, P.A.F., Kusznir, N.J., & iSIMM Team, 2008. Lower-crustal intrusion on the North Atlantic continental margin, *Nature,* **452,** 460–464.

Wilkens, R.H., Fryer, G.J. & Karsten, J., 1991. Evolution of porosity and seismic structure of upper oceanic crust: importance of aspect ratios, *J. geophys. Res.,* **96**(B11), 17 981–17 995.

Zelt, C.A. & Smith, R.B., 1992. Seismic traveltime inversion for 2-D crustal velocity structure, *Geophys. J. Int.,* **108,** 16–34.

SUPPORTING INFORMATION

Additional Supporting Information may be found in the online version of this article:

Supplement. This document contains supplementary material to the main article, documenting the complete wide-angle seismic data set, interpretation, ray tracing models and traveltime fit.

Please note: Wiley-Blackwell are not responsible for the content or functionality of any supporting materials supplied by the authors. Any queries (other than missing material) should be directed to the corresponding author for the article.